2012

Linear-cavity tunable fibre lasers employing an Opto-VLSI processor and a MEMS-based device

David Daniel Michel
Edith Cowan University

Edith Cowan University

Copyright Warning

Linear-cavity tunable fibre lasers employing an Opto-VLSI processor and a MEMS-based device

David Daniel Michel 2023663

Bachelor of Engineering (Communications)/

Bachelor of Science (Computer Science)

Faculty of Computing, Health and Science

August 2012

Abstract

This thesis proposes and demonstrates experimentally two novel linear-cavity tunable fibre lasers employing an erbium-doped fibre (EDF) in conjunction with an Opto-VLSI processor and a MEMS-based device for wavelength selection. The Opto-VLSI processor and the MEMS-based device along with an optical collimator, a Bragg grating plate and an optical lens, enable the realisation of an optical filter for continuous tuning of wavelengths over the amplified spontaneous emission (ASE) range of the EDF.

We also propose the use of a section of un-pumped EDF as a saturable absorber (SA), which suppresses noise spikes caused by the high optical pumping power. Experimental results show that by optimising a length of the SA a single wavelength, high power laser signal can be achieved.

In addition, we experimentally demonstrate that the performance of the proposed linear-cavity tunable fibre lasers is better than that of ring-cavity tunable laser counterparts. Specifically, we show that linear-cavity based tunable fibre lasers can achieve higher output power, a larger side mode rejection ratio (SMRR) and narrower laser linewidth than ring-cavity tunable fibre lasers.

Declaration

I certify that this thesis does not, to the best of my knowledge and belief:

i. Incorporate without acknowledgment any material previously submitted for a degree or diploma in any institution of higher education;

ii. Contain any material previously published or written by another person except where due reference is made in the text of this thesis; or

iii. Contain any defamatory material;

Acknowledgements

I would like thank my principal supervisor Prof. Kamal Alameh and associate supervisor Dr. Feng Xiao who have given me their time and shared their vast “lake” of knowledge throughout my time at ESRI. Without their continual support and guidance, this Master degree would not have been successfully completed. In particular, I would like to thank Prof. Kamal Alameh for giving me the opportunity to study in ESRI, where staff and students are continually supported to grow both personally and professionally.

I would also like to thank the administration staff at ESRI, past and present, (Linda Arthur, Beverly McKinnon, Tiella Turkovic and Paul Roach). They never hesitated to help, in their area of expertise, to maintain the “family” like spirit within ESRI.

Finally, ESRI would not be the same with all of the students proceeding from their different nationalities. This has created an environment where one can learn and enrich his/her personal life while at the same time having made friendships that will certainly last a life time.

Table of Contents

Chapter 1

Lasers and Laser Types

1.1 Introduction

In this chapter, the concept of lasers and the different types of lasers is presented by describing their main characteristics. The most widely used laser types include semiconductor lasers, gas lasers and fibre lasers. Two novel tunable fibre lasers using a linear-cavity structure with an Opto-VLSI processor and a MEMS-based device are proposed. The concept of user generated holograms is described as the main mechanism for the Opto-VLSI processor and the MEMS-based device to enable wavelength selection. These tunable fibre laser structures are the main research topic investigated experimentally, where Opto-VLSI processor and the MEMS-based device are electronically re-configured to select specific wavelengths for lasing.

1.2 The Concept of Lasers

The word laser stands for the acronym Light Amplification of Stimulated Emission by Radiation. Stimulated emission in a two-level laser system, which is illustrated in Fig. 1, is the phenomenon that leads to optical amplification, whereby the interaction of a photon with an electron that is already in an excited state that matches the energy gap between the excited and ground states of that electron, stimulates the emission of an additional photon that is in phase with the stimulating photon, thus leading to photon amplification. Therefore, by exciting electrons from the ground state to the excited state an optical gain medium can be established. The essential components required to realise a laser are:

1. An optical gain medium, which may be solid crystals, e.g. ruby or Nd:YAG, liquid dyes, gases like CO2 or Helium/Neon, semiconductors such as GaAs or rare-earth-doped optical fibres such as erbium-doped optical fibres. Optical gain media contain atoms whose electrons may be excited to a meta-stable energy level by an energy source.

2. An excitation mechanism, where external pump energy is applied into the optical gain medium by basic methods: optical, electrical or chemical.

3. A high reflectance mirror, which ideally reflects 100% of the laser light.

4. A partially transmissive mirror, which reflects less than 100% of the laser light and transmits the remainder.

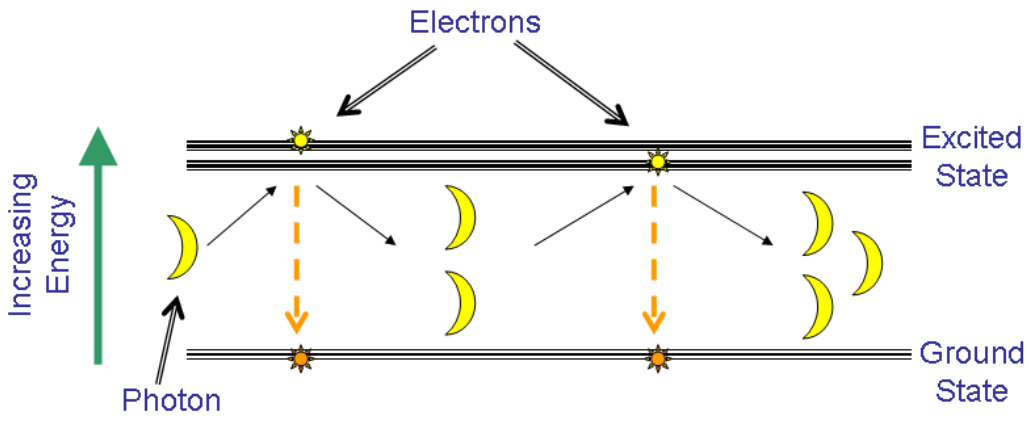

Figure 1. Diagram illustrating the stimulated emission which creates additional photons when an electron in an excited energy state interacts with a photon which matches the energy gap that the electron experiences from the excited state to the ground state.

The first reported laser in the literature was created by Theodore Maiman in 1960 and a representation diagram is shown in Fig. 2. This laser in particular was able to create pulses of light from a cylindrical shaped ruby crystal with two mirror surfaces on either side, where a high intensity light source was coiled around the ruby crystal. When the high power light source discharged its energy onto the ruby crystal, the photons from the light source interacted with the ruby crystal electrons, raising their potential energy. As the ruby crystal electrons fell back to a lower energy level, photons of light were emitted by the electrons leading to an amplification effect inside of the ruby crystal. Once enough photons were produced, some escaped the ruby crystal and emitted pulses of light with wavelengths in the visible red region.

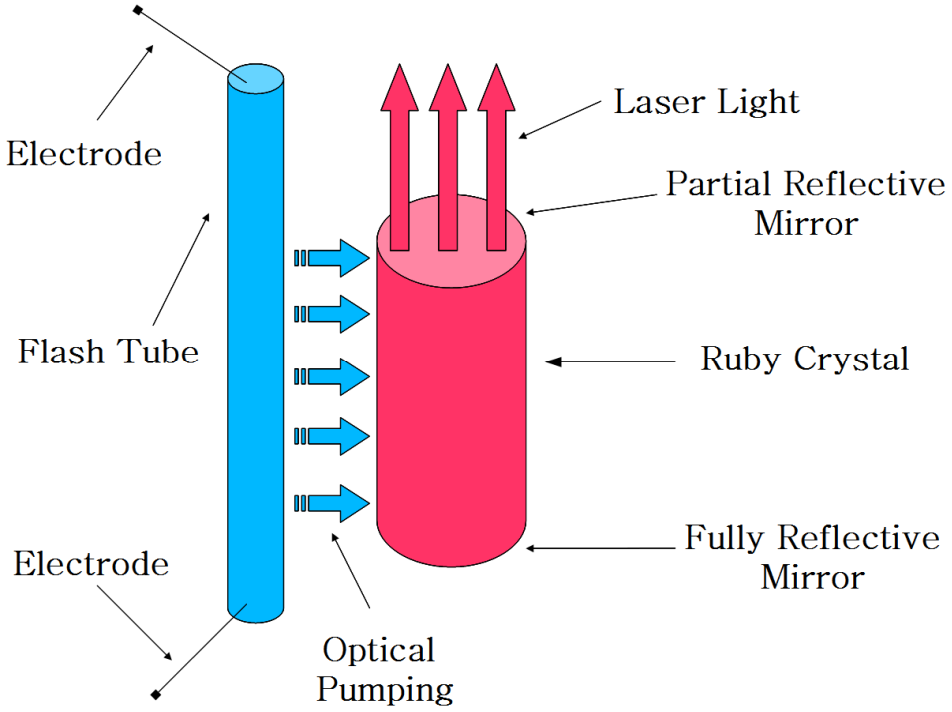

Figure 2. Diagram representing a ruby laser where a ruby rod externally pumped by flash tube and two silver mirrors create a resonator cavity to produce a laser beam.

The idea that atoms were capable of emitting light resulted from the experimental evidence that molecules could emit microwave radiation. Certain number of experiments from Columbia University in New York and from Lebedev Institute in Moscow showed that microwave amplified by stimulated emission of radiation (MASER) was possible, resulting in the Noble Prize for science contribution in 1964 to be awarded to Dr. Townes, Dr. Basov and Dr. Prochorov.

Laser light tends to travel spatially in a narrow beam as an electro-magnetic (EM) wave that propagates with small change of its phase characteristics. Amplification occurs due to the light wave being reflected inside of a resonant or amplifying cavity created by using two highly reflecting surfaces as illustrated in Fig. 3. This is done by using highly reflective mirrors which allow the light to propagate inside the cavity multiple times. As the light energy begins to build up in the cavity, some of the light energy or photons escape through one of the reflective cavity ends, which is slightly less reflective than the mirror at the opposite side of the cavity.

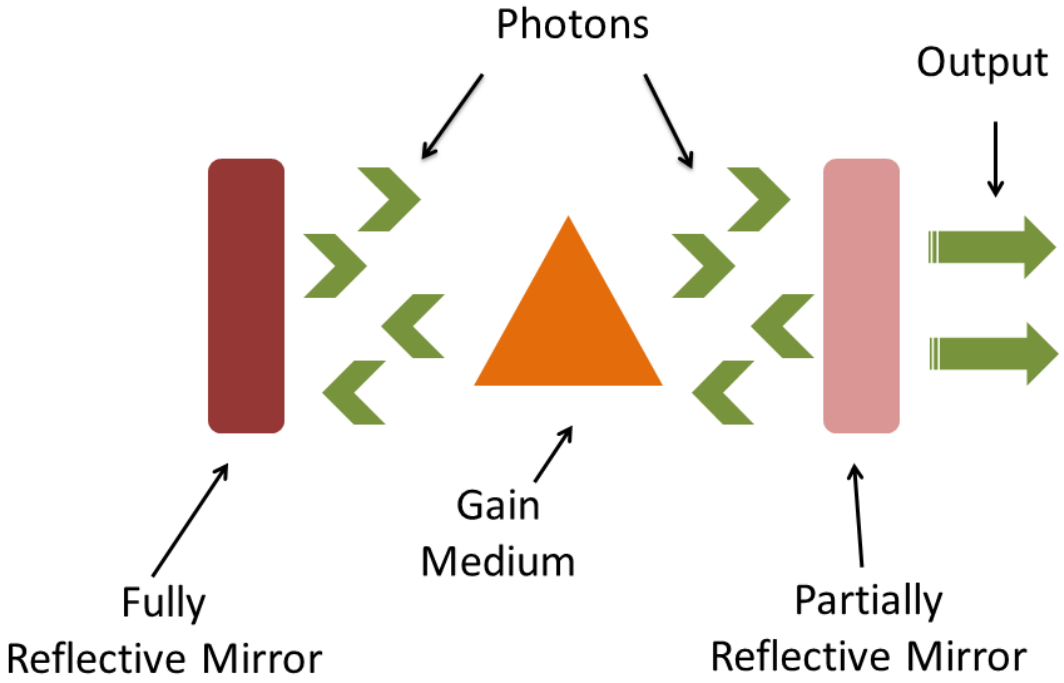

Figure 3. Diagram illustrating an optical cavity with highly reflective mirrors as cavity ends where photons of light build up inside the optical cavity.

The atomic energy levels for erbium atoms is shown in Fig 4, where photons in either the 1480 nm or 980 nm ranges are used as optical energy pumps which can be absorbed by the erbium atoms, raising electrons to a higher and sometimes unstable energy level. These electrons spontaneously decay to a lower energy meta-stable state. A population inversion is achieved when the majority of erbium electrons are energised into a meta-stable state. Laser action then occurs when an electron spontaneously returns to its ground state, resulting in a photon of light. When the energy from this photon is of a precise wavelength matching the energy level of another excited electron, the photon stimulates the production of another photon of the same wavelength and phase, resulting in a cascading effect. The highly-reflective and partially reflective mirrors continue the reaction by directing photons back through the gain medium along the horizontal axis of the laser cavity. The partially reflective mirror allows a small amount of coherent radiation to exit the laser cavity which is observed as a laser beam. Laser radiation continues as long as the pump energy is applied to the optical gain medium to produce amplified spontaneous emission (ASE) of photons with a wavelength in the 1550 nm range.

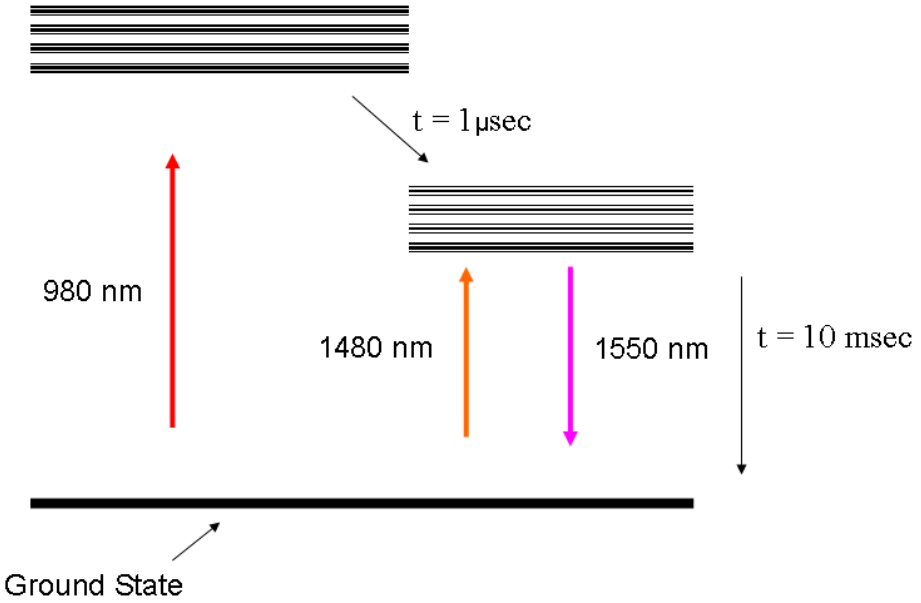

Figure 4. Atomic energy levels for an erbium atom where photons in either the 1480 nm or 980 nm ranges used as optical energy pumps are absorbed by the erbium atom to produce ASE of photons with wavelengths in the 1550 nm range.

Other important aspects of laser beams are spatial and temporal coherence, which relate to the characteristics of the EM wave over time and space, as illustrated in Fig. 5. Usually laser beams have a high degree of spatial coherence which relates to the electric field values at different distances along the beam of laser light. When a beam has a well defined relationship between the electric field at different points in space, it is called spatially coherent. Furthermore, when the electric field at a constant point in space can be described by a sinusoidal wave, then a laser beam is said to have high temporal coherence.

Figure 5. Diagram of the orthogonal phase characteristics of an EM wave illustrating the spatial and temporal coherence and the visual representation of one wavelength. Las Cumbres Observatory Global Telescope Network. (2012)

The term that is used to characterise the spectral shape of a laser signal is called linewidth. The linewidth describes the width of a lasing wavelength at its full width at half maximum (FWHM) or commonly referred as the 3 dB point from the maximum amplitude as shown in Fig. 6. There are numerous applications which require the use of narrow linewidth lasers such as spectroscopy, fibre sensors and for scientific measurement control.

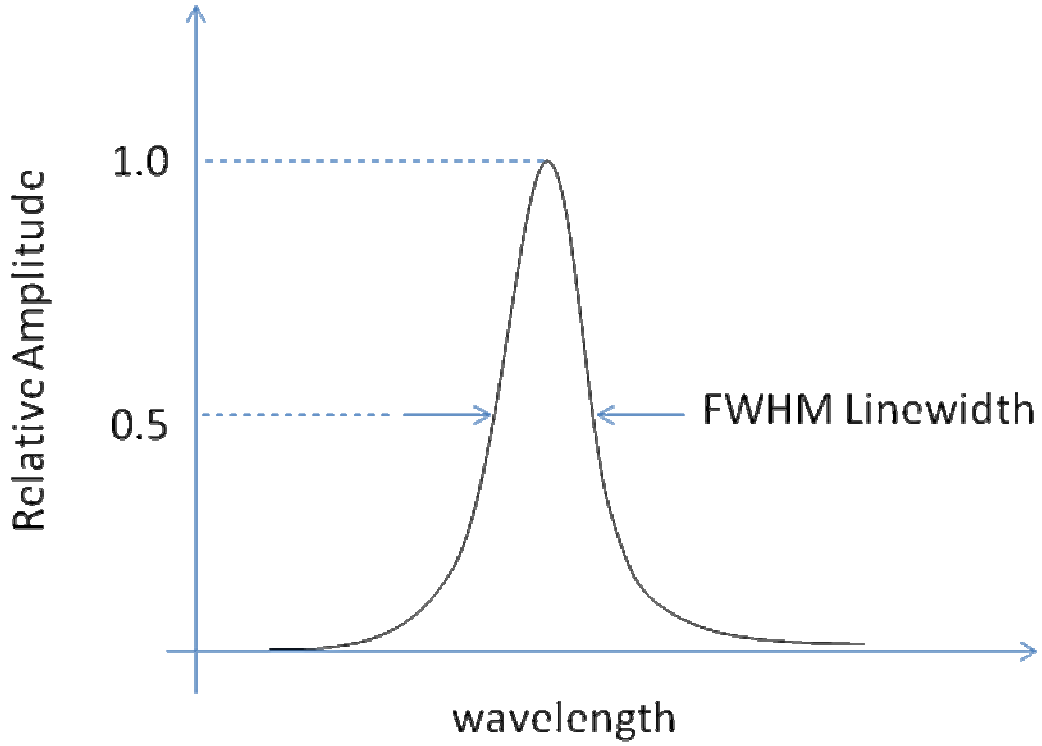

Figure 6. Diagram illustrating the linewidth of a Lorentzian beam measured at the FWHM or 3 dB point.

Several methods are used to determine the linewidth of a laser, depending on the size of the linewidth to be measured. If the expected linewidth is more than 10 GHz, optical spectrum analysis based on using diffraction gratings can be used efficiently. Otherwise, self-heterodyne techniques must be utilised if the laser linewidth to be measured is in the kHz range.

The self-heterodyne technique involves the splitting of a laser signal into two parts. One of these is made to travel along a longer length of fibre than the other beam. The two beams are later combined and detected by a single photo-detector. The beam that travels the shortest path is made to pass through a phase shifting device such as an acousto-optic modulator. The purpose of the elongated length of the fibre is to introduce a time delay between the two split signals. When both laser signals are recombined and detected by the photo-detector, they will produce an electrical signal with a beat which can be used to measure the linewidth of the original laser beam. This process is necessary because optical signal frequencies are too large to be measured by current electronic technologies.

1.2.1 Semiconductor Lasers

Semiconductor lasers are generally manufactured with inorganic materials like gallium arsenide, indium phosphide, or gallium nitride to name a few. These lasers are based on electrically pumping electrons from the valance band up to the conduction band, and when the electron from the conduction band recombines with the hole created in the valance band, a photon of light is released. This photon of light has the same energy value corresponding to difference in the electron's energy state from the conduction band down to the valance band. It is also possible to force an electron to jump to the conduction band by the use of a photon whose energy is slightly higher than the band gap, which is the energy measured from the valance band up to the conduction band. Figure 7 illustrates the layered structure of a forward-biased semiconductor laser diode where the active region behaves as a resonant cavity and the laser light beam exits the device on the edge of the laser diode.

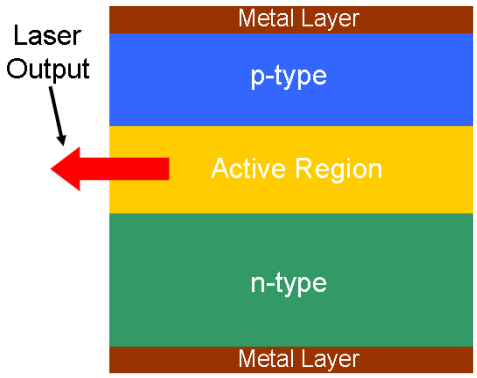

Figure 7. Diagram showing the structure of a laser diode composed of two metal layers, a p- and n-type regions and the active layer where the surface edge of the laser diode is the output of laser light.

The great majority of semiconductor lasers are known as laser diodes. To force a laser diode to create a beam of light, the p-doped and n-doped regions are electrically pumped, causing electrons to move to higher energy states, as mentioned earlier. There are different types of laser diodes, namely edge-emitting, external cavity, and surface emitting lasers - also known as vertical cavity surface emitting lasers (VCSELs). Some common applications for edge-emitting lasers include optical storage, laser pointers or in fibre optic communications. These lasers tend to output high quality laser beams with average powers of a few milliwatts.

External cavity laser diodes are used in a cavity which is longer than the device itself. This is achieved by coating one end of the laser diode with a highly reflective surface which creates a mirror and the opposite end acts as the output for the laser diode. The output from the laser diode is then collimated using a lens and a diffraction grating can be used to make the laser diode tunable over a range of wavelengths. The diffraction grating becomes the other reflective cavity end needed to create a laser resonator cavity. Due to their inherited small laser linewidth, these external cavity laser diodes tend to be used in spectroscopy for characterisation of gases.

VCSELs are one of the most recent types of laser diodes and an illustration is shown in Fig. 8. These lasers have a manufacturing advantage over other types of laser diodes since a single device can be comprised of many individual laser diodes. VCSELs have become predominant in the communications field especially in the 850 nm range where transmission between devices within a distance of 50 m is required. Other areas of interest include the use of VCSELs with plastic optical fibres (POFs) and also through free space in wireless optical networks.

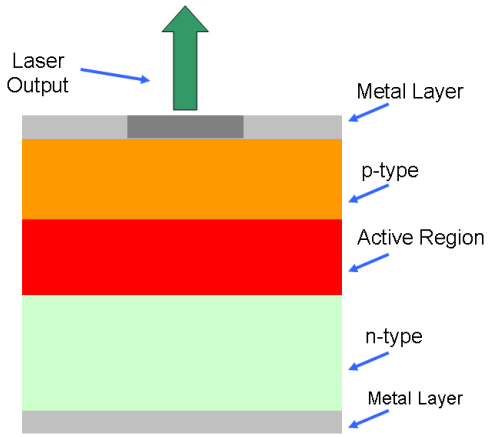

Figure 8. Diagram showing the structure of a VCSEL composed of two metal layers, a p- and n-type regions and the active layer where the output of laser light is emitted through a gap (area in dark grey)from the top layer.

1.2.2 Gas Lasers

The gain media used in gas lasers is normally a mixture of elements in their gaseous state such as helium (He) and neon (Ne). For gas lasers to create a beam of laser light, a resonator cavity is needed where an external energy source, pumping source, is used to excite the gas inside of the resonator cavity to create a population inversion of the gas element in question. The resonator cavity tends to be created by the use of highly reflective mirrors and once there is enough energy build up inside of the cavity, a portion of this energy escapes through one of the two mirrors as a laser beam. In Fig. 9, a schematic diagram of a carbon dioxide (CO_2) laser is presented, which illustrates the main components required to create a gas laser, namely an external pumping source, a resonator cavity and a gain medium.

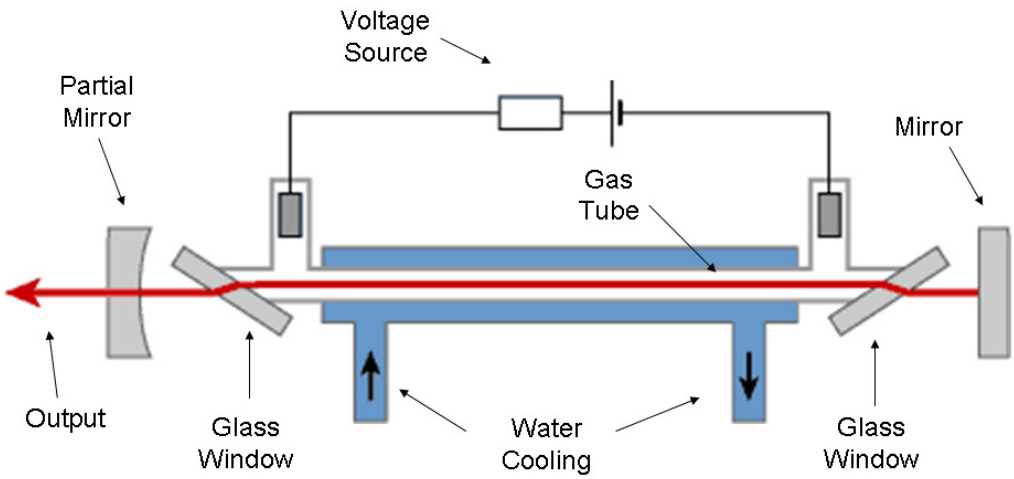

Figure 9. Schematic representation of a CO_2 laser where the red arrow represents a laser beam of light and the blue section is water cooling for the gas inside of the resonator cavity (space between the two glass windows). An electrical potential difference is created between each end of the cavity mirrors by an external voltage source, (see top part of figure), creating an electrical discharge inside of the cavity. Paschotta, R. (2011)

Gas lasers have several attractive properties, namely (i) they provide laser beams with high beam qualities due to weak distortions in their optical properties, (ii) they enable the realisation of laser sources with an output wavelength not readily achievable like that produced by CO_2 lasers, (iii) they have the ability to produce laser beams with high output powers, sometimes measured in the kilowatt range, and (iv) they are also able to deal with heat management better than other laser sources such as laser diodes. Some of the most common wavelengths produced by gas lasers are 632 nm for visible red coloured He-Ne lasers, 514 nm visible green coloured Argon lasers, and longer infra-red wavelengths of 10.6 µm for CO_2 lasers.

1.2.3 Fibre Lasers

The invention of a low power loss optical fibre by Corning Inc, paved the way for fibre optic communications to reach several kilometres before any need of signal regeneration. At first, semiconductor lasers were used as the light source but an important problem occurs when trying to couple the light into an optical fibre since much of the light is lost due to the small core diametre of optical fibres. On the other hand, fibre lasers do not have any loss due to coupling since the light is generated inside of the optical fibre itself as illustrated in Fig. 10.

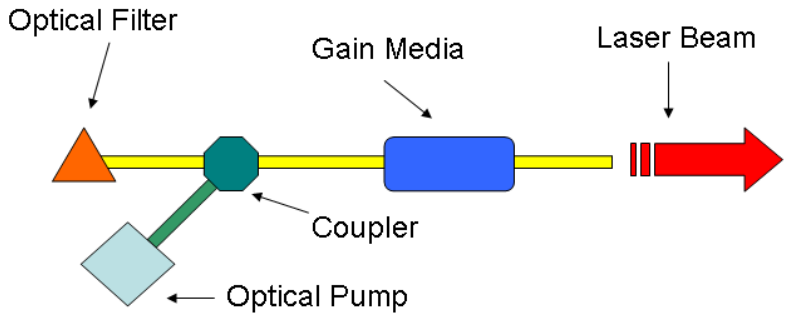

Figure 10. Illustration of a fibre laser employing a linear-cavity where the laser beam exits via a cleaved optical fibre.

Other benefits of fibre lasers include (i) easy manufacture without the need of clean rooms and expensive device packaging; (ii) compatibility with fibre-optic communication systems, mechanical flexibility and the ability to withstand bending; (iii) broadband gain spectrum and high energy efficiency; high laser beam quality, ensuring their wide potential applications in material processing, printing, marking, cutting and drilling; (iv) robustness, because all

optical signals are guided within optical fibres, thus eliminating the need for optical alignment; and (v) narrow linewidth, due to their long cavity lengths, which is essential for many applications and hard to achieve for their current semiconductor laser counterparts.

Fibre lasers are created by adding or doping into the fibre core rare earth elements such as erbium or ytterbium. When the optical fibre with these elements is optically energised or pumped it produces ASE, which in the case of EDFs, results in an ASE with a range of wavelengths from 1530-1560 nm. The section of optical fibre that contains a doping element is known as the optical gain medium, and this becomes the source of the laser light amplification. In fibre lasers, the gain medium can be used in conjunction with either a ring-cavity resonator or a linear-cavity resonator shape.

1.3 Tunable Fibre Lasers

The term tunable fibre lasers refers to the ability of a fibre laser source to change or select a specific wavelength of light being emitted from the resonator cavity as illustrated in Fig. 11. Normally tunable fibre lasers select a wavelength for lasing from the broadband ASE produced when the gain media is optically pumped, and when one of these wavelengths is selected, the output changes accordingly. The wavelength selection is achieved by changing the length of the resonator cavity or by filtering unwanted wavelengths, which then allows a different wavelength to experience gain and amplification. There a number of techniques used to realise tunable fibre lasers such as using acousto-optic filters, spatial light modulators, etalon based filters such as Fabry-Pérot filters, etc.

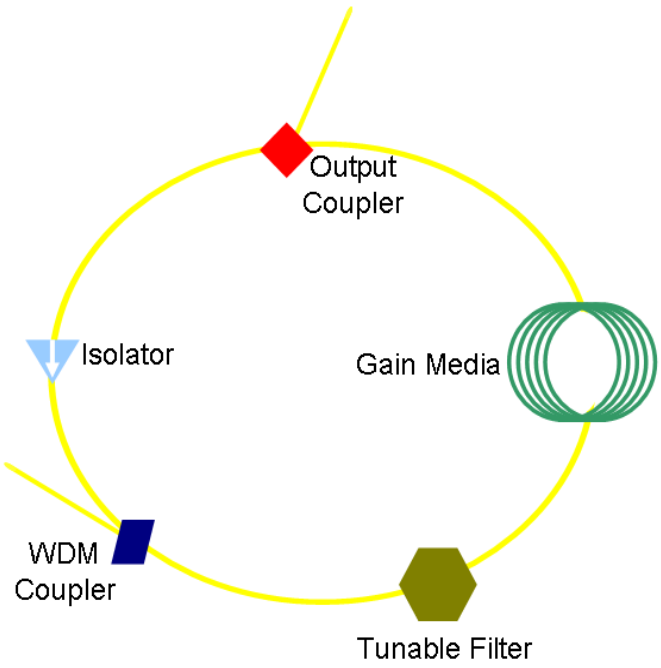

Figure 11. Diagram illustrating a tunable fibre laser which employs a ring-cavity geometry. Wavelength tunability is realised by the use of a tunable filter were a portion of the ASE is used for amplification to produce lasing for the required wavelength.

Tunable fibre lasers have many application areas, including spectroscopy, optical device characterisation, optical sensing, and optical fibre communications. Spectroscopy is the science of being able to detect the spectral characteristics of atoms or molecules. This is performed by analysing the transmission or absorption spectra of the element under analysis. Since different elements have diverse spectral characteristics, a laser source with the ability to output different wavelengths is required to accurately sense or characterise the substance under investigation.

Optical components must be characterised over a wide spectral range before they are integrated into an optical system, and this characterisation requires high-resolution tunable lasers to accurately characterise the integrated optical system. In optical communications especially where fibre optics are used, the wavelength division multiplexing technique (WDM) allows for multiple wavelengths to share one optical fibre. This requires a tunable laser source capable of synthesising arbitrary wavelength channels, each is used for carrying data along the optical fibre.

1.3.1 Linear-Cavity Based Fibre Laser Structure

Fibres lasers based on the use of a linear-cavity structure require two cavity ends to create a laser resonator. Some techniques to achieve this are by using highly reflective fibre ends or by using fibre loop mirrors. In Fig. 12, a fibre laser developed with a linear-cavity is shown were the resonator cavity is achieved by using a fibre mirror and an optical filter, each creating a reflecting cavity end. One of the main benefits which a linear-cavity has over a ring-cavity fibre laser is that the lasing wavelength will pass through the gain media twice per cycle. This makes the gain medium reach deep saturation, whereby the spectral shape of the output power over the whole ASE range becomes flat, meaning that the output power differs by very small values. Linear-cavity fibre lasers also have the advantage over ring-cavity fibre lasers of achieving higher output power levels [1]. Furthermore, ring-cavity fibre lasers tend to be more complex in structure due to the need of additional components inside of the resonator cavity [2].

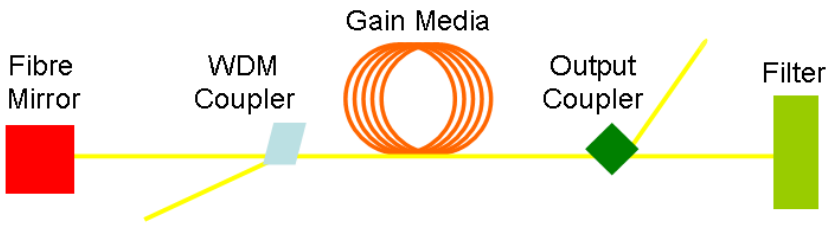

Figure 12. Fibre laser developed with a linear-cavity structure composed of an optical filter, an output coupler, an amplifying gain medium and a WDM coupler to enable optical pumping of the gain medium.

Fibre lasers with linear-cavities experience a phenomenon called spatial hole burning (SHB). This is due to the interference caused by two energy waves travelling in opposite directions inside of the linear resonator cavity. These two waves interfere constructively with each other, causing a change in the gain characteristics of the erbium-doped fibre amplifier (EDFA) gain medium. This results in rapid mode hopping that causes the fibre laser output wavelength to fluctuate [3]. The wavelength instability can be minimised by incorporating into the linear-cavity fibre laser a section of un-pumped EDF which to act as a saturable absorber, reducing the fluctuations from the fibre laser output.

1.3.2 Ring-Cavity Based Fibre Laser Structure

Fibre lasers developed with a ring-cavity allow only one direction of travel for the lasing wavelength. Figure 13 illustrates a fibre laser with a ring-cavity structure with an optical filter for wavelength selection. The benefit of this is to eliminate the SHB effect which affects the EDFA characteristics. The realisation of a single travelling wave direction is accomplished by incorporating an optical circulator or isolator into the ring-cavity structure. Since ring-cavity fibre lasers also have long cavity lengths, unstable laser operation is often encountered, were the output wavelength mode hopes over the many available densely spaced wavelength modes [4]. The optical filter used for laser tuning must be able to discriminate successfully between the numerous longitudinal modes [5]. Narrow-band Fabry-Pérot filters can solve this issue, however, they require non-conventional tuning mechanisms and thus they are relatively expensive.

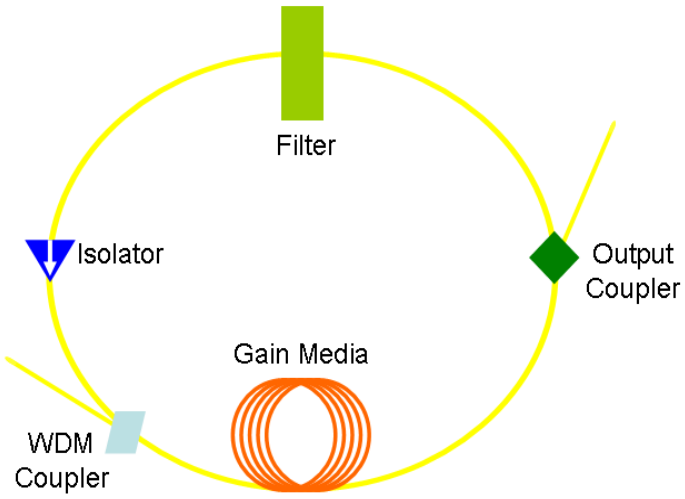

Figure 13. Fibre laser developed with a ring-cavity structure composed of an optical isolator, an optical filter, an output coupler, amplifying gain medium and a WDM coupler for optical pumping.

1.4 Proposed Tunable Fibre Laser Employing a Linear-Cavity Structure

This thesis primarily focuses on linear-cavity-based fibre lasers because of two key advantages, namely, (i) simple system architecture, and (ii) the ability to use the EDFA gain media to operate in deep saturation mode. The developed tunable linear-cavity fibre laser comprises a number of components and devices, as shown in Fig. 14. The wavelength tunability of the laser is achieved by choosing specific optical components which enable an Opto-VLSI processor or a MEMS device to select an appropriate wavelength from the available broadband ASE and re-injecting the selected wavelength into the linear cavity to realise lasing. Three optical components which include a fibre collimator, a lens and a Bragg plate in conjunction with an Opto-VLSI processor, or a MEMS device, realises as the optical filter used in the proposed tunable fibre lasers.

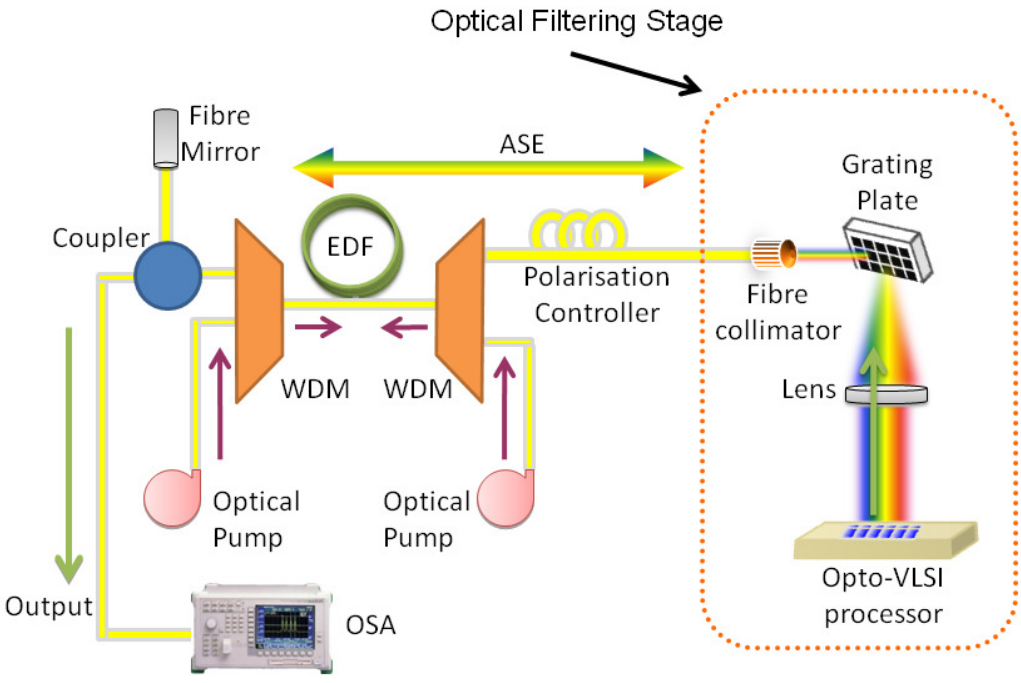

Figure 14. Fibre laser structure developed with a linear-cavity. System tunability is realised by the use of the novel optical filtering stage (dashed orange line).

The gain medium selected for this system has been an erbium doped fibre (EDF) whose optical spectrum emission corresponds to the C-band of optical telecommunications with a wavelength range between 1530-1560 nm. The ASE matches the nearly transparent window of optical fibres, thus enabling an optical signal within the C-band to travel through optical fibres with minimum attenuation of approximately 0.2 dB/ km [6].

In order to create ASE from the gain medium, two laser diode pumps were utilised which produced optical energy in the 980 nm wavelength region. The energy from these two optical pumps was coupled into the resonator cavity by using two WDMs. ASE produced by the excitation of the EDF by the optical pumps' energy travelled in a forward and backward direction. The two ASE waves reflected off a fibre mirror and the Opto-VLSI processor or the MEMS device to create a linear-cavity structure.

For the tunable fibre systems to accomplish wavelength selection, user-generated holograms were created on a PC and uploaded to the MEMS device or an Opto-VLSI processor's active window. The role of the hologram is to select a portion of ASE energy that is incident upon the Opto-VLSI processor back into the gain medium for further amplification. The Opto-VLSI processor is dynamically reconfigurable to select any wavelength within the bandwidth of the ASE. An example of a hologram used in a MEMS device for wavelength selection is shown in Fig. 15.

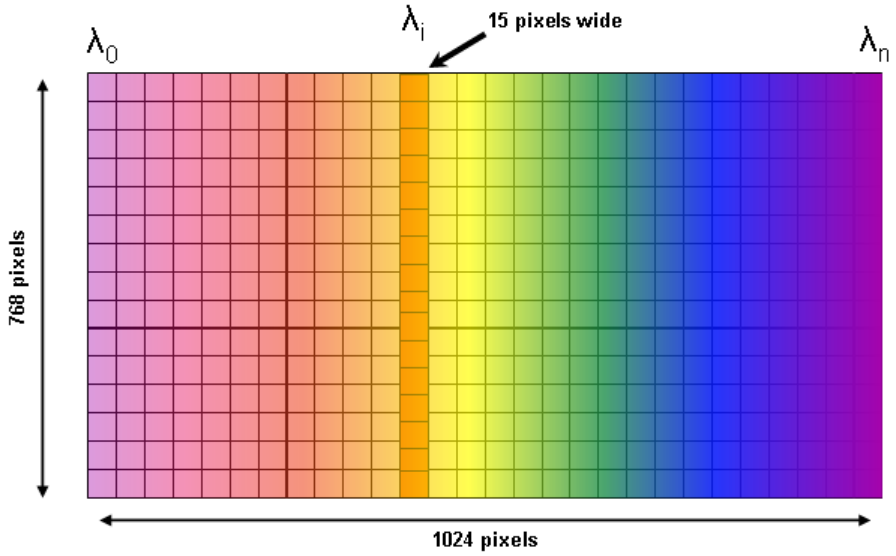

Figure 15. Representation of a hologram depicted on MEMS device, where the section in orange, is a group of micromirrors used for re-injection of wavelength into the fibre cavity for lasing.

1.5 Conclusions

In this chapter, a description of the concept of lasers has been presented by describing their main characteristics. The most commonly used types of lasers have also been discussed, namely semiconductor lasers, gas lasers and fibre lasers. Tunable fibre lasers have been described by showing the two types of optical resonator gain shapes used which was a ring- or linear-cavity structure. The architectures of the proposed tunable fibre lasers using a linear-cavity structure in conjunction with either a MEMS-based device or an Opto-VLSI processor have been presented. The concept of user-generated holograms was presented as the main method that the MEMS device and the Opto-VLSI processor employ for selecting a portion of the ASE of an EDFA for lasing through multiple optical amplifications.

Chapter 2

Key Laser Components

2.1 Introduction

In chapter 1, the most commonly used lasers were presented by describing their main characteristics. The overall system architecture of the proposed tunable fibre lasers using a linear-cavity structure were shown and described. In this chapter, the system block structure of the proposed tunable fibre laser is presented, and its main optical components are described in detail.

2.1.1 System Overview of Proposed Tunable Fibre Laser using a Linear-Cavity Structure

This thesis experimentally demonstrates the increase in performance characteristics of using a linear-cavity structure over ring-cavity geometry to realise a tunable fibre laser. The main system components used in the experimental procedures are shown in Fig. 16. The linear-cavity is created by the use of two reflective components, a fibre mirror and an optical filter, which enable a resonant cavity with an optical gain medium to be realised. The amplification of the lasing signal takes place in the gain medium and an optical pump is therefore required to continuously supply energy to the gain medium for the increase in energy of the chosen wavelength for lasing by using a wavelength division multiplexer (WDM) coupler. An optical coupler is used to tap into the resonator cavity for signal monitoring by an optical spectrum analyser (OSA). In order to connect all of the optical components together, single mode optical fibre patch cables are utilised.

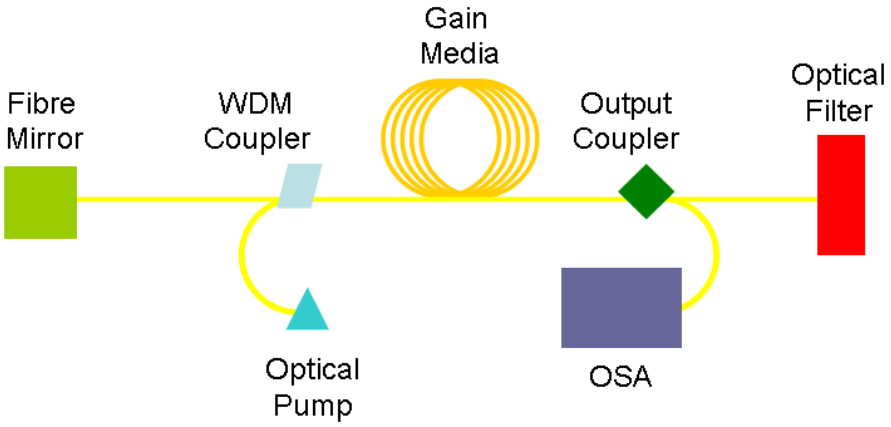

Figure 16. Illustration of the main coponents proposed in the tunable fibre laser using a linear-cavity structure.

2.2 Optical Fibre

2.2.1 Main Benefits

Light has the ability to transmit more data and allows for a larger bandwidth than electricity since the bandwidth of a system is directly proportional to its frequency spectrum. The frequency of light waves for an optical system tend to be measured in the 10^{14} Hz range while for an electrical system are measured in the 10^{9} Hz range for gigabit networks. This difference equals many orders of magnitude more which correspond to higher capacity for data transfer [7].

Another important advantage optical systems have over electronic is the immunity from electromagnetic interference or radio frequency interference, due to the fact that an optical fibre is a wave guide. Even if multiple fibres carrying a single wavelength are bundled together, no cross talk can occur. When adding the fact that optical fibres can have very low attenuation losses, the reduction of the number of repeaters or amplifiers needed for successful transmission enables the cost of the system and maintenance to decrease significantly [8].

2.2.2 Optical Fibre Structure

An optical fibre is made of several layers which are illustrated in Fig. 17. The inner layer is named the core and consists of pure silica with the addition of impurities or dopants such as zinc sulphide. Surrounding the core is another layer called cladding and is also made out of silica but also contains other compounds or dopants. The refractive index of the fibre can be controlled by varying the amount of dopants present in either the core or the cladding. In order to protect the brittle core and cladding layers, another layer covers these which is called buffer. The buffer is created to help the optical fibre to absorb mechanical stress and to add flexibility to the optical fibre. Normally the final layer that protects all of the previous layers is called the jacket and is made out of plastic.

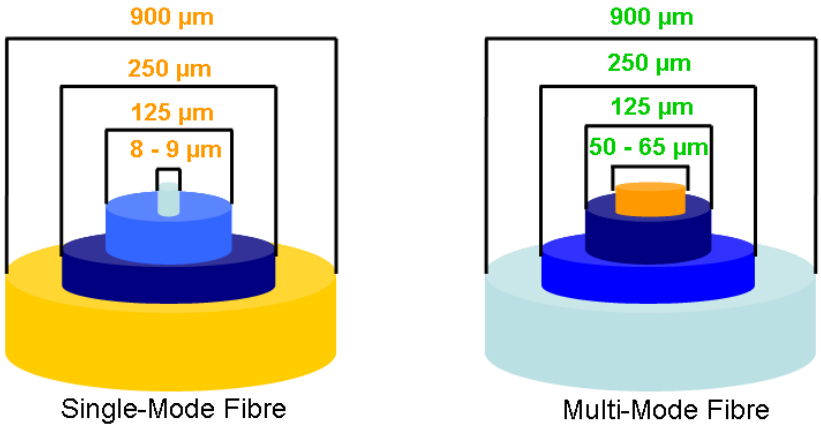

Figure 17. Diagram representing the physical differences between single-mode and multi-mode optical fibres.

2.2.3 Transmission Modes of an Optical Fibre

In terms of optical communications, data is sent over optical fibres by launching laser light into one of the ends of the optical fibre. The light then travels along the fibre as shown in Fig. 18, by the use of either single- or multi-mode optical fibres. The difference between these two types of fibres is related to the internal structure of the optical fibre which determines the allowed transmission modes for the light to propagate along the fibre. For single mode fibres, the size of the core is normally measured to be around 9 µm and allows only one electro-magnetic (EM) mode to travel through the core of the fibre. However, the size of the core in multi-mode fibres is in the range of 50 - 62.5 µm which allows multiple EM modes to propagate along the fibre, hence enabling more data to be sent on a single fibre, however only over short transmission distances, mainly because of their high attenuation.

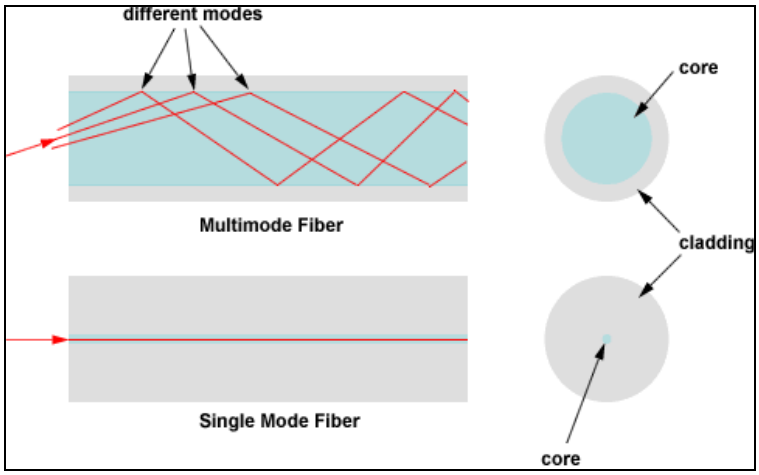

Figure 18. Transmission modes in single- and multi-mode fibres where the main physical difference is the diametre size of the core.

2.3 Opto-VLSI Processor

2.3.1 Opto-VLSI Processor

An Opto-VLSI processor is an electronic reconfigurable device capable of generating phase holograms that cause a beam of light to experience beam steering. Beam steering is performed by creating a ramp phase grating which corresponds to a periodic ramp phase pattern produced by driving the pixels of the Opto-VLSI processor with different voltage levels. Once a phase hologram is designed in software, it is then uploaded onto the Opto-VLSI processor resulting in beam steering. Since Opto-VLSI processors have no moving parts, any possible vibrations experienced by the device will not affect its operation.

The principle behind beam steering is illustrated in Fig. 19, through a prism, which steers an incident light beam by an angle that depends on the value of the prism's angle. By increasing the physical size of a prism's angle, a light beam which travels through the prism will experience a larger steering angle due to the phase change of the light beam as it exits the prism, since portion B of the light beam travels much less time through the prism than portion A, as shown in Fig. 19 (b).

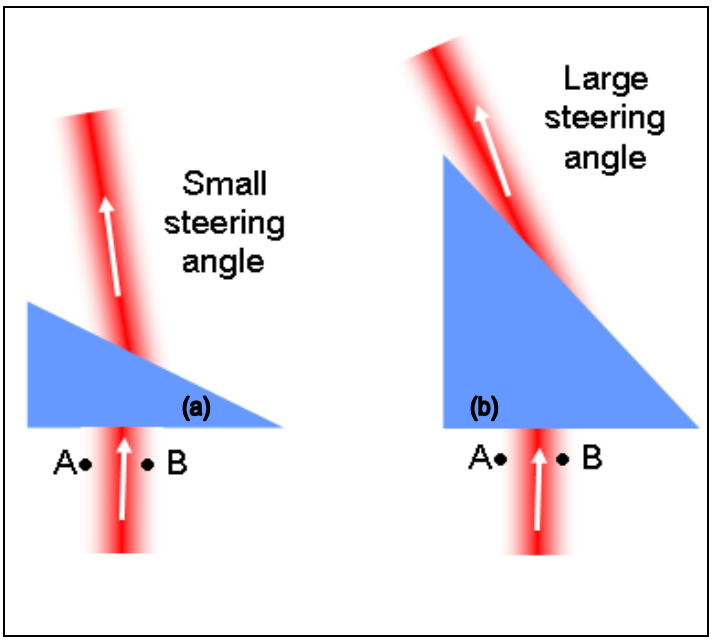

Figure 19 (a). A light beam travelling through a prism experiences a small steering angle corresponding to the size of the prism's angle. (b). An increase in the steering angle is experienced by a light beam when the size of the prism's angle is larger.

As mentioned earlier, the phase hologram resembles a grey scale ramp which is also periodic in nature. All phase holograms utilised during the experimental procedures have been generated using an algorithm especially developed with the aid of the Lab-View software package. This program is able to interface with the Opto-VLSI processor to individually reconfigure each of the pixel's state, thus realising a phase grating that enables the cross-section of the incoming light beam to experience the appropriate phase shift necessary to steer it along arbitrary directions as shown in Fig.20. The phase hologram can be uploaded onto the Opto-VLSI processor via an electronic driver linking the Opto-VLSI processor to the computer running the software interface.

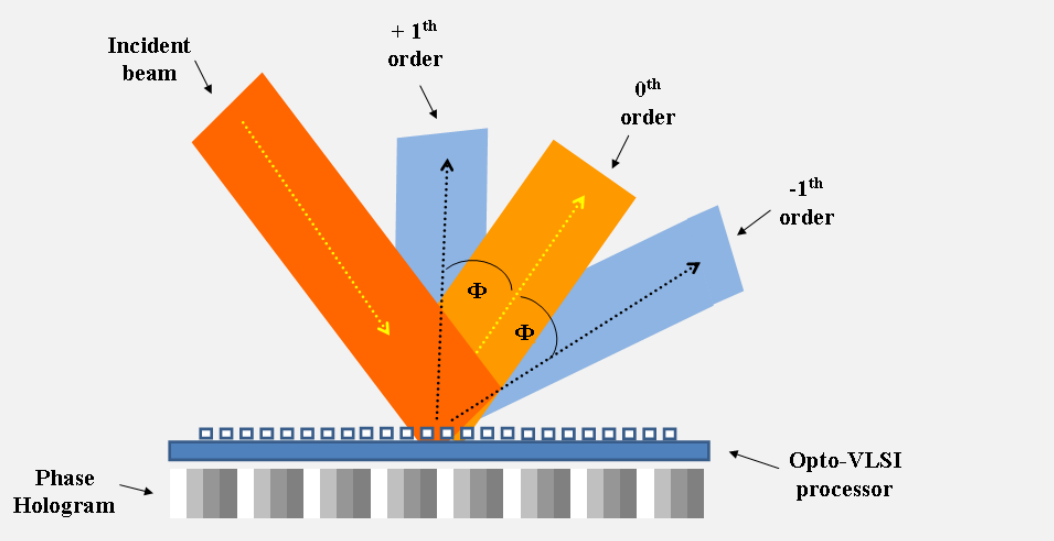

Figure 20. Illustration of an incident light beam interacting with an Opto-VLSI processor with a phase hologram which is created with a software program developed with the Lab-View package. The software is designed to upload a phase hologram to the Opto-VLSI processor. The hologram is periodic and realises a blaze grating where an incident light beam experiences a change in its reflected angle, also known as beam steering.

As stated earlier, the hologram generation is performed via the aid of a user interface program developed using the Lab View software package. This program has the ability to control all 262,144 pixels of the Opto-VLSI processor utilised in the experiments, and change the 256 brightness levels of any pixel to create high-resolution phase holograms. Figure 21 shows a screen capture of the software interface for the Opto-VLSI processor. A number of sections are available for the user to interact with. Starting from the top of Fig. 21, the 1st button creates the hologram image on the PC, the 2nd button sends the image from PC to the PCI control board, the 3rd button sends the hologram image to the front window of the Opto-VLSI processor, and the 4th button is used to disconnect the connection between the PC and the Opto-VLSI processor. The remaining sections are to change the pixel phase level and location, the preview window is for the location of the phase hologram on the front window of the Opto-VLSI processor and the main paths used by the user interface to store the hologram into the PC.

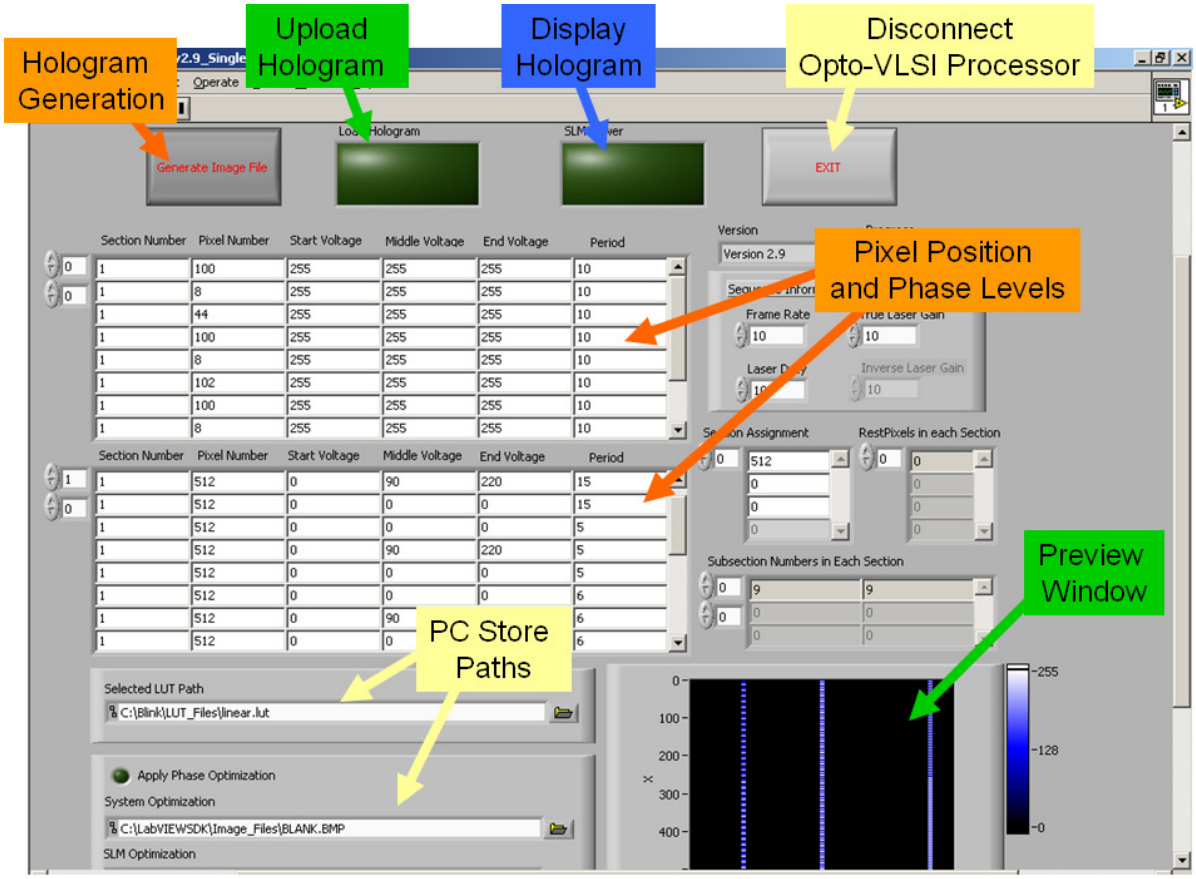

Figure 21. A PC screen capture of the user interface program which allows user generated holograms to be created, generated, previewed and uploaded to the Opto-VLSI processor.

When the periodicity of a phase grating profile is changed, the beam steering angle also changes accordingly. For example, an increase of the phase grating periodicity, shown in Fig. 22 (a), results in an increase of the beam steering angle experienced by a light beam which is represented by the two points A and B as illustrated in Fig. 22 (a). In Fig. 22 (b), an incident light beam experiences beam steering when a phase hologram is uploaded onto the Opto-VLSI processor. Depending on the profile characteristics of the phase hologram, the beam steering experienced by the light beam can be changed.

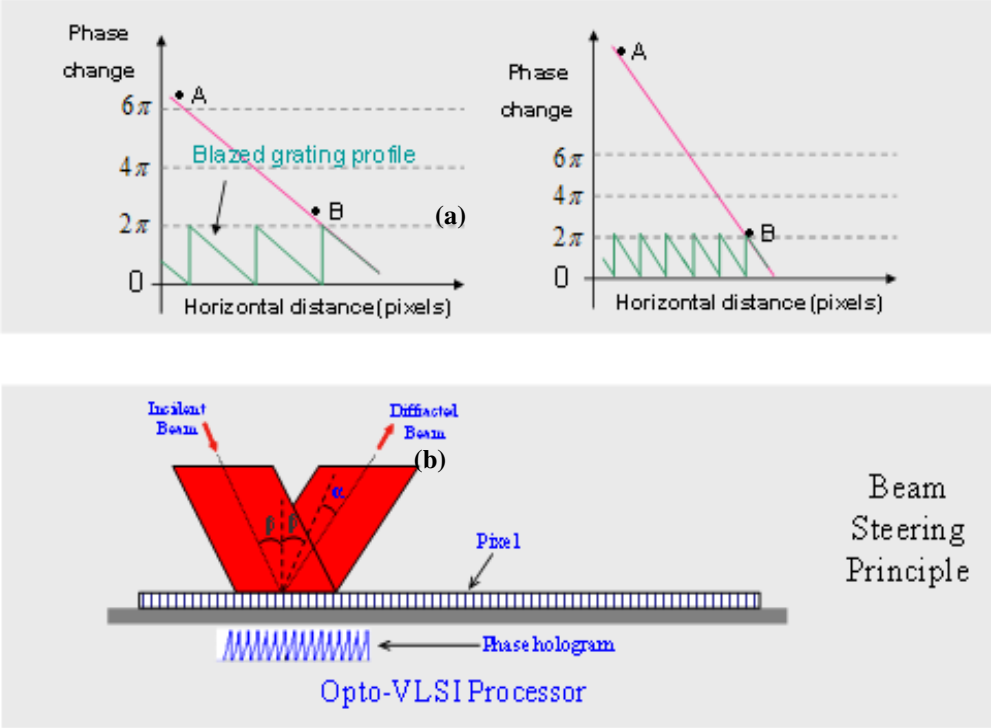

Figure 22 (a). Different phase grating periods correspond to different beam steering angle. (b). An incident light beam experiences a spatial phase change when a phase hologram is uploaded onto the Opto-VLSI processor.

The periodicity of the phase hologram and the beam steering angle are related by the fact that as the period of the phase hologram is increased the beam steering angle experienced by an incoming light beam also increases. For a small incidence angle, the maximum steering angle of the Opto-VLSI processor is given by:

$$\theta_{\max} = \frac{\lambda}{M \cdot d} \quad (1)$$

In Eq. 1, M is the number of phase levels, d is the pixel size, and λ is the wavelength. For example, a 4-phase Opto-VLSI processor having a pixel size of 5 microns can steer a 1550 nm laser beam by a maximum angle of around ±4°. The maximum diffraction efficiency of an Opto-VLSI processor depends on the number of discrete phase levels and it is given by [9]:

$$\eta = \mathrm{sinc}^2\left(\frac{\pi n}{M}\right) \quad (2)$$

In Eq. 2, $n = gM + 1$ is the diffraction order ($n = 1$ is the desired order), and g is an integer. For an Opto-VLSI processor with binary phase levels ($M = 2$) it can have a maximum diffraction efficiency of 40.5%, while a 4-phase-level Opto-VLSI processor can attain an efficiency of up to 81%. The higher diffraction orders (which correspond to the cases $g \neq 0$) are typically unwanted crosstalk signals, which can be attenuated or routed outside the output ports to maintain a low-noise performance.

The Opto-VLSI processor can be realised to function as a wavelength selection device, when the individual wavelength channels of a WDM signal are separated by using a Bragg plate and then a lens is used to focus the light on the front window of the Opto-VLSI processor as illustrated in Fig. 23. Once the WDM signal is mapped onto the Opto-VLSI processor, via the Bragg plate, any WDM channel can either be reflected back, via beam steering, into the optical fibre or steered off track so that it is not coupled into the input optical fibre. By changing the phase hologram profile, different steering angles can be realised. The use of a fibre collimator, a Bragg plate, a lens and an Opto-VLSI processor produces a device which behaves like an optical filter.

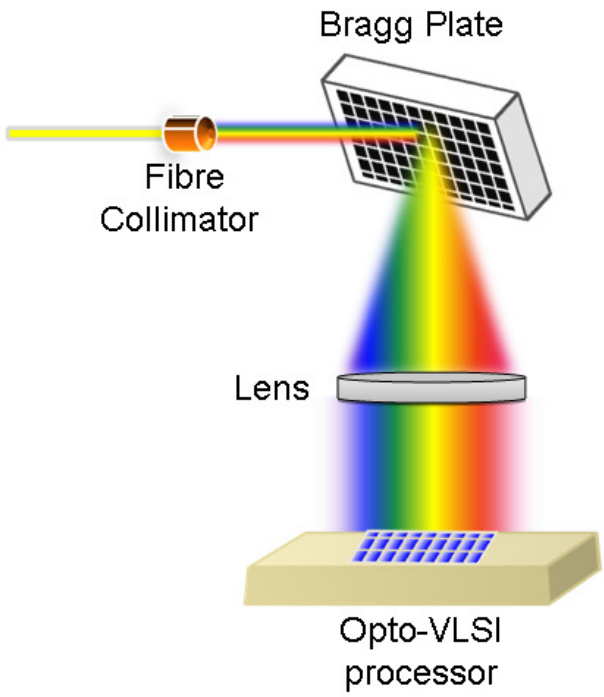

Figure 23. Illustration of wavelength selection using an Opto-VLSI processor in conjunction with various optical components to realise an optical filter.

It is important to note that the Opto-VLSI processor technology has several unique features when it is used for tuning the laser wavelength. It allows (i) independent tuning of each wavelength channel, (ii) arbitrary control of the power level for each wavelength channel, (iii) the generation of wavelength channels over various operation ranges, (iv) sufficient maximum continuous wave power output per channel (> +10 dBm), (v) adequate laser linewidth (i.e. comparable to performance by Agilent of less than ±0.001 nm at 1550 nm), and (vi) low power fluctuations (< 0.01 dB over 10 hours). These features are far superior to all tuning mechanisms reported in the literature to date.

2.3.2 Layout of Opto-VLSI Processor

An Opto-VLSI processor is an electronic reconfigurable device comprising an array of liquid crystal (LC) cells driven by a Very-Large-Scale-Integrated (VLSI) circuit that generates digital holographic diffraction gratings to steer and/ or shape optical beams. Each pixel is assigned a few digital memory elements, and a multiplexer that selects one of the input voltages and applies it to an aluminium mirror electrode. The Opto-VLSI processor is electronically controlled, configured via software, polarisation independent and cost effectively produced through mass fabrication. It is also very reliable since beam steering is achieved with no mechanically moving parts. Figure 25 shows a typical layout and a cell design of an N-phase Opto-VLSI processor. An Indium-Tin Oxide (ITO) film is used as the transparent electrode, while evaporated aluminium is used as the reflective electrode. The ITO layer is generally grounded and a voltage is applied at the reflective electrode through the VLSI circuit below the LC layer.

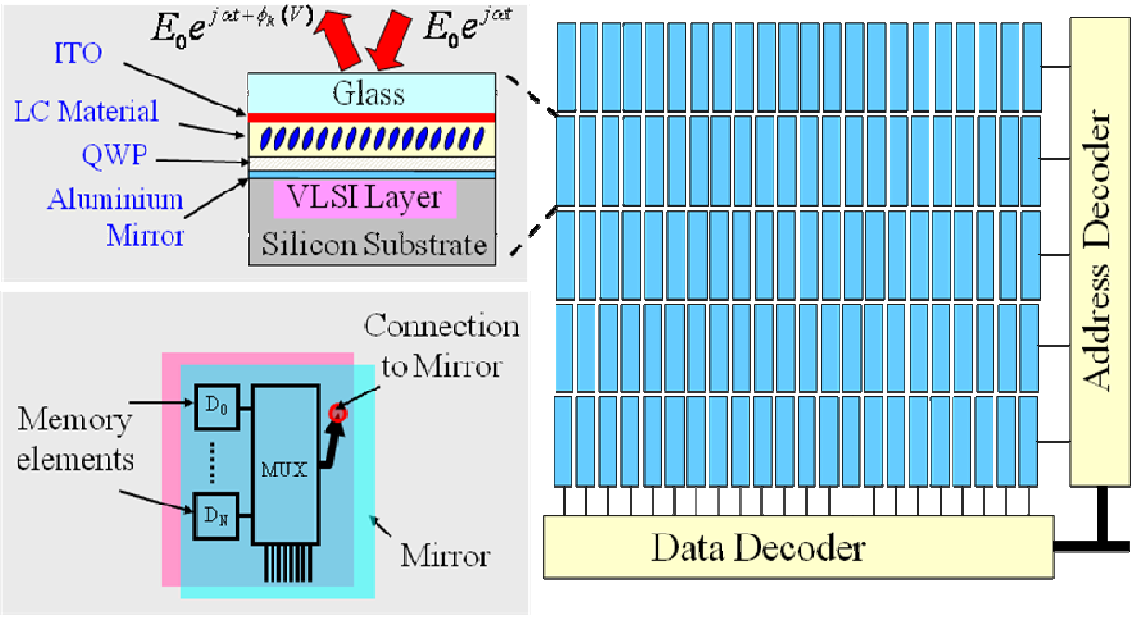

Figure 25. Diagram illustrating a typical N-phase Opto-VLSI processor and the LC cell structure design.

Adaptive optical beam steering can be achieved by reconfiguring the phase hologram uploaded onto the Opto-VLSI processor. Recent advances in low-voltage nematic LC materials and layer thickness control have enabled the incorporation of a thin quarter-wave-plate (QWP) layer between the LC and the aluminium mirror to accomplish polarisation-insensitive Opto-VLSI processors [10], as shown in Fig. 25. In addition, with current 90 nm VLSI fabrication processes, VLSI chips featuring 24 mm × 24 mm active area, maximum switching voltage below 3.0 volts, and pixel size as small as 5 microns, can be realised.

Various algorithms have been reported for the optimization of Opto-VLSI phase holograms to achieve arbitrary beam steering, including simulated annealing and projection methods. In this project, simulated annealing was employed for generating phase holograms for accurate beam steering with low crosstalk. An electronics driver is used to drive the Opto-VLSI processor circuitry thus enabling individual addressing of all the pixels. For the Opto-VLSI processor used in the experiments, each pixel had a total of 262,144 pixels (512 × 512), and 256 different phase levels (8 bits) with the pixel pitch (distance between two adjacent pixels) measuring 15 μm.

The first step in creating a phase hologram is to use the user interface to drive each pixel to the necessary state. Once the phase hologram has been created, it is then uploaded to the Opto-VLSI processor via a peripheral component interconnect (PCI) card which connects directly from a personal computer (PC) to the electronic driver, as shown in Fig. 26. Connecting the Opto-VLSI processor via the PCI interface allows the transfer of 8 bit, 512 × 512 pixel images from the PC in approximately 6.6 ms [11]. The refresh rates can be programmed with a range from 1 Hz up to 1 kHz, although frequencies below 1 kHz are best suited for the current application for the Opto-VLSI processor.

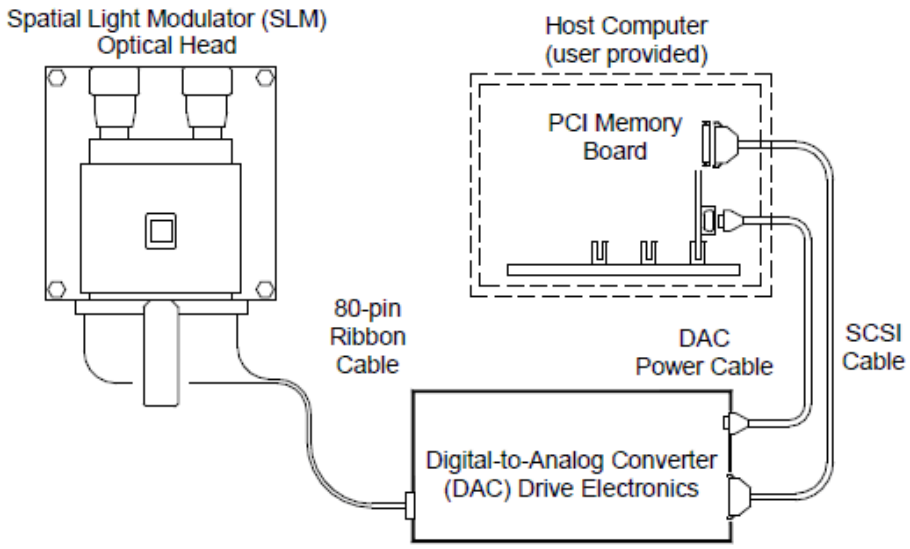

Figure 26. Schematic diagram showing how the Opto-VLSI processor is connected to the electronic driver and to the PC for uploading user generated phase holograms.

2.3.3 Applications of Opto-VLSI Processors

Opto-VLSI processors have a number of application areas that can benefit from their unique features, including optical filters, adaptive optics, laser scanning, WDM equalisers, photonic RF signal processing, tunable lasers and reconfigurable optical add-drop multiplexers (ROADMs). Xiao, F., et al., [12], successfully demonstrated the ability of an Opto-VLSI processor to realise, in conjunction with other photonic and opto-electronic components, a microwave photonic transversal filter with positive and negative coefficients. A further application area where an Opto-VLSI processor was utilised is in tunable fibre lasers [13], where the Opto-VLSI processor was used as an optical filter for wavelength selection and re-injection into a fibre ring-cavity, leading to laser signal generation over the available

amplified spontaneous emission (ASE) produced by an erbium-doped fibre (EDF). A further example that demonstrates the capability of Opto-VLSI processors is the ROADM reported in [14], where the Opto-VLSI processor was used in conjunction with off-the-shelf optical components to dynamically add or drop WDM channels as well as equalise their power levels over the entire C-band of optical communications.

2.4 Micro-Electro-Mechanical System (MEMS) Device

2.4.1 Micro-Electro-Mechanical System (MEMS) Device

In this thesis, a MEMS device was also used as one of the optical filter components due to its unique feature of being able to individually and precisely control the tilt angle of micromirrors. The MEMS device enables WDM wavebands within the ASE of an erbium-doped fibre amplifier (EDFA) to be selected and re-injected into the EDFA cavity for lasing. MEMS devices have typically a small micromirror pitch (distance between two adjacent micromirrors) thus allowing fine tuning resolution to be realised [15].

The MEMS device used in the experiments was made by Texas Instruments and it is supplied as part of the DLP Discovery 4100 Development kit, which comprises a Digital Micromirror Device (DMD), a digital controller, a DMD power and reset driver. A typical layout of the MEMS device is illustrated in Fig. 27, which comprises vias, micromirrors, hinges, yokes, landing tips, electrodes and a CMOS VLSI circuit. The CMOS VLSI circuit where the memory cells are located is created on a silicon substrate. Each micromirror can have three different states, or tilt angles, corresponding to 0°, and ±12°, which can be selected via binary coding of the VLSI circuitry.

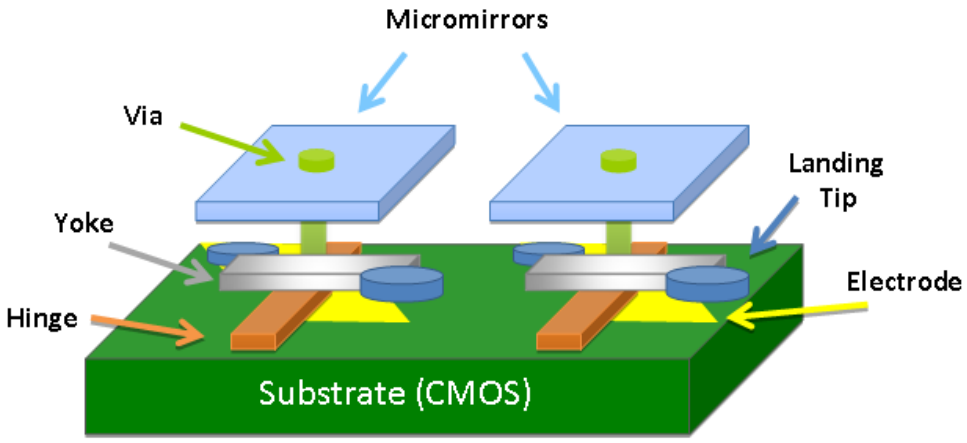

Figure 27. Layout of a MEMS device comprising micromirrors, vias, hinges, yokes, landing tips, and electrodes, all built on a CMOS VLSI circuit.

The CMOS VLSI circuit is comprised of memory cells as shown in Fig. 28. The tilt angle of a micromirror is controlled by loading the appropriate logic value into the memory location corresponding to that micromirror. As mentioned earlier, to change the tilt angle of the micromirror a reset command must be activated after the logic value has been loaded onto the corresponding memory location.

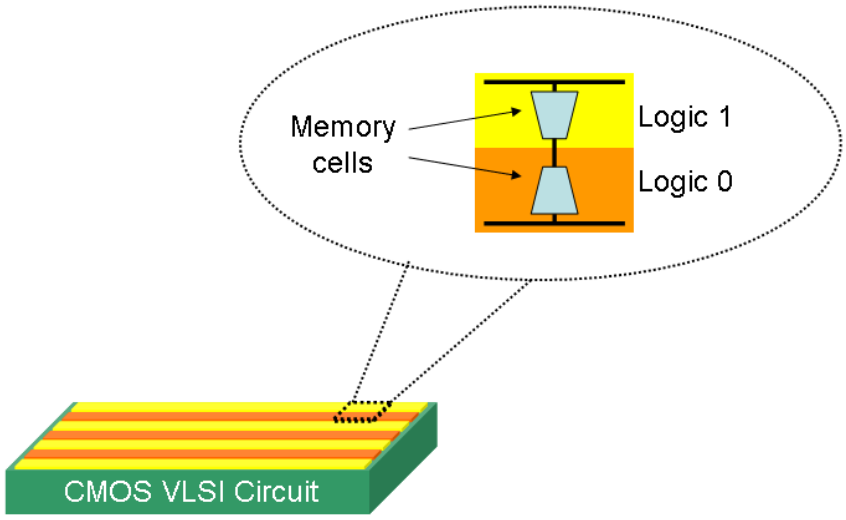

Figure 28. Illustration of the CMOS VLSI circuit structure which controls the tilt direction of each micromirror.

The active window of the MEMS array is 11.1 × 8.3 mm, which consists of 1024 × 768 micromirror elements. The size of each individual micromirror element is 10.8 × 10.8 µm, and was especially selected because of its small micromirror physical size and excellent reflectivity (~ 97 %) in the near infra-red (NIR) spectrum.

The micromirrors allow the individual control of each micromirror via software and a digital CMOS VLSI circuit, which steers and holds the individual micromirror elements along predefined directions. Each micromirror is attached through one via to the yoke underneath the micromirror. A hinge is used to allow the yoke to pivot in a diagonal axis once the appropriate signal has been applied to the MEMS device coming to a rest on the landing tip. The steering or tilting of the micromirrors is controlled with an electro-static force between the yoke and the electrode and the direction of tilt is determined by the state of the 1-bit memory cell under each micromirror. The voltage of the SRAM cell determines whether the micromirror stays at its current position or changes its tilt angle. However, the voltage state of the memory cell does not change the tilt angle of the micromirror automatically. A reset command is sent to the MEMS device where the micromirrors are allowed to detach from their landing tips, in which they return to a floating state when the electro-static force has been removed. If the logic memory cell voltage is changed from the previous logic state, from 1 to 0 or 0 to 1, an electro-static force switches the micromirror tilt angle to the opposite state. Otherwise, if the logic voltage value of the memory cell remains constant, the micromirror re-tilts to its original tilt angle before the application of the reset command.

It is important to note that holographic data storage based on MEMS devices have the potential to save data in an optical medium with storage densities greater than the current storage densities of magnetic and existing optical discs. In order to resolve digital holograms, the MEMS device must be able to attain good light throughput characteristics and appropriate diffraction efficiencies. MEMS devices are excellent candidates for applications requiring high contrast, broad spectral bandwidth and high diffraction efficiencies [16].

2.5 Conclusions

In this chapter, the generic architecture for the proposed linear-cavity tunable fibre laser systems has been presented. The main components used in the tunable fibre laser have been described in detail, especially the main characteristics of optical fibres, and the key reconfigurable components, namely the Opto-VLSI processor and the MEMS device.

Chapter 3

Tunable Fibre Lasers – Literature Review

3.1 Introduction

In Chapter 2, the proposed linear-cavity tunable fibre laser system architecture was introduced and the main components utilised were described including an overview on the main characteristics of optical fibres, the Opto-VLSI processor and the MEMS-based device. In this chapter, a review of the scientific literature is presented, describing the reported techniques used to achieve tunable fibre lasers employing ring- or linear-cavity structures.

3.1.1 Benefits of Using Lasers

Lasers have been used in many applications and industries including information and communications technology (ICT), health, agriculture, security, defence and environment. Some examples of laser applications include optical transmitters, DVD players, printers, surgeries, heat treatment, spectroscopy, surveying, laser pointers, welding and nuclear fusion. In particular, lasers have revolutionised the optical telecommunications through the development of cost effective high-speed fibre-optic communication links, enabling through the use of wave division multiplexing (WDM), faster data transmission and high data throughputs in the order of Tb/s (10^{12} bits/sec) per optical fibre.

Cost-effective information transmission would not have been possible without lasers, and particularly, tunable lasers. In particular, tunable fibre lasers, which employ optical fibre cavities and a gain medium, have recently attracted great interest owing to many unique advantages over traditional semiconductor lasers, including, (i) easy fabrication without the need of clean-rooms and expensive device packaging, (ii) mechanical flexibility and the ability to withstand bending, (iii) broadband gain spectrum and high output power capability, (iv) high laser beam quality, (v) robustness, as the optical signal is well guided within the optical fibre, thus eliminating the need for optical alignment and (vi) narrow linewidth. Benefiting greatly from recent developments in fibre communications, fiber lasers can offer a low-cost alternative to traditional semiconductor laser counterparts. In this thesis, we demonstrate a new viable tunable laser source featuring both reduced cost and hardware

complexity in addition to delivering equivalent or improved performance in comparison to commercially-available tunable laser counterparts.

3.2 Tunable Fibre Lasers Employing Linear-Cavities

So far tunable fibre lasers employing erbium-doped fibres (EDFs) are based on the use of either ring- or linear-cavities, wherein the gain medium is embedded. Fibre lasers employing a linear-cavity can be understood as a length of optical fibre acting as the gain medium, having been doped with rare earth elements, with two highly reflective surfaces on either side of the optical fibre, thus creating a resonant cavity as illustrated in Fig. 29. For a fibre laser to become tunable, additional optical components are required to be introduced into the linear-cavity resonator for wavelength filtering or selection.

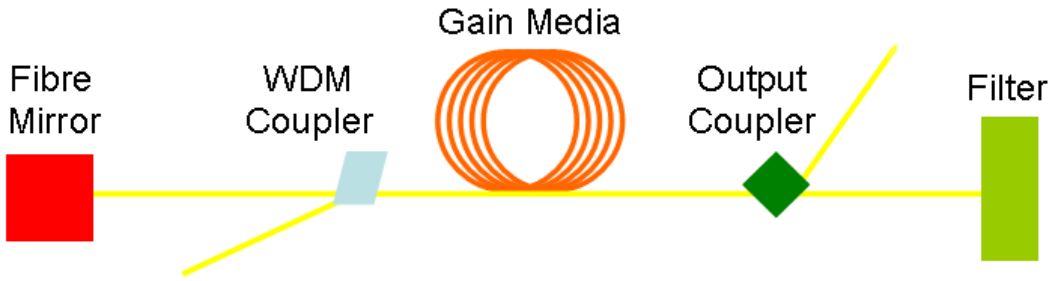

Figure 29. Typical structure of a tunable fibre laser employing a linear-cavity geometry.

In terms of the number of publications, ring-cavity based tunable fibre lasers outnumber linear-cavity based tunable fibre lasers [17]. The most common tunable optical filters reported in the literature for tunable fibre lasers with linear-cavities are fibre Bragg gratings (FGBs) [18-20], etalon based filters or Fabry-Pérot cavities [21-22] and acousto-optic based tunable filters [23]. These tunable optical filters are necessary since the longer the laser cavity the more difficult it is to control multi-mode laser oscillation, which results in multiple lasing wavelengths very closely spaced from each other, thus decreasing the linewidth of the laser's output [24]. Since FBGs are susceptible to environmental conditions, a change in temperature causes the stability of an FBG-based tunable laser to degrade. As a result, higher costs are involved in the manufacturing process of tunable fibre lasers in order to improve their stability. In addition tunable etalon based filters require complex manufacturing processes to

become compatible with fibre-optic components, and this increases their cost and makes them impractical [24].

The previously mentioned optical filters have also been employed in conjunction with other optical components in order to further improve the tuning capability and performance of tunable fibre lasers. For example, the use of a 20 nm band-pass optical filter in conjunction with a tunable fibre Fabry-Pérot (FFP) filter has been reported for wavelength filtering and tuning [25], shown in Fig. 30. While utilising two wavelength filtering devices produced arbitrary wavelength tuning over a 20 nm bandwidth, further extending the tuning range was difficult since the tuning range of the FFP filter was 28 nm.

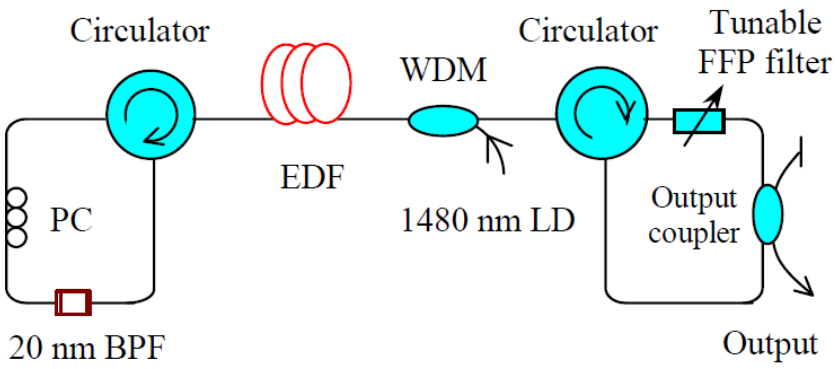

Figure 30. Diagram illustrating a linear-cavity based tunable fibre laser employing a band-pass filter for bandwidth selection and a tunable FFP filter for wavelength selection [25].

Another example where a combination of optical components was reported to create a tunable fibre laser with a linear-cavity is reported in [23], and a schematic diagram of such a tunable fibre laser is illustrated in Fig. 31. For this tunable laser, an acousto-optic filter was used in conjunction with a saturable absorber (SA) which acted as a narrow band Bragg filter for stable single wavelength lasing. The acousto-optic filter was operated by shifting the optical wave frequency to stop the formation of a standing wave patter inside of the gain medium. Figure 31 shows that the optical frequency was shifted down at the acousto-optic tunable filter 1 (AOTF 1) and shifted up at the acousto-optic tunable filter 2 (AOTF 2) by a particular frequency (fA). Furthermore, a saturable absorber was utilised to suppress the mode-hopping effect which prevented single longitudinal mode operation.

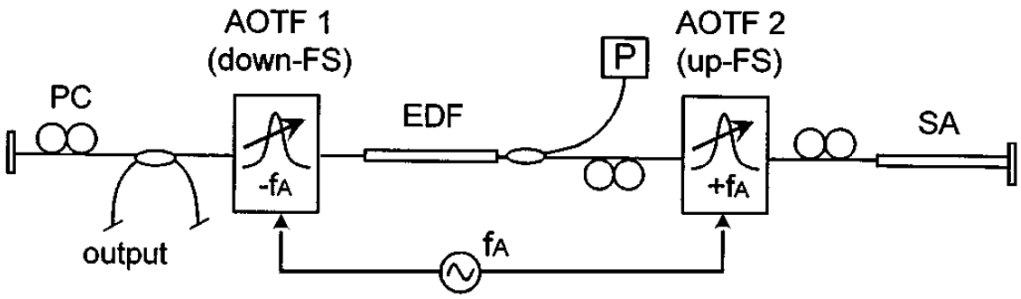

Figure 31. Illustration of a linear-cavity based tunable fibre laser employing acousto-optic filters in conjunction with a SA. The tunability of the fibre laser is accomplished by modifying the modulation frequency of the acousto-optic filters (by using AOTF1 and AOTF2) and a SA to realise single longitudinal mode wavelength lasing [23].

3.3 Tunable Fibre Lasers Based on Ring-Cavities

Numerous ring-cavity based tunable fibre laser structures have been reported [26-28], however, an interesting structure is that reported in [26] where the combination of a stretchable FBG and a SA resulted in a tunable fibre laser structure shown in Fig. 32, with a tuning range exceeding 40 nm. By stretching the FBG, a specific wavelength is reflected back into the laser cavity for lasing. Also, the SA acted as a very narrow band optical filter that suppressed mode hoping and allowed single mode operation.

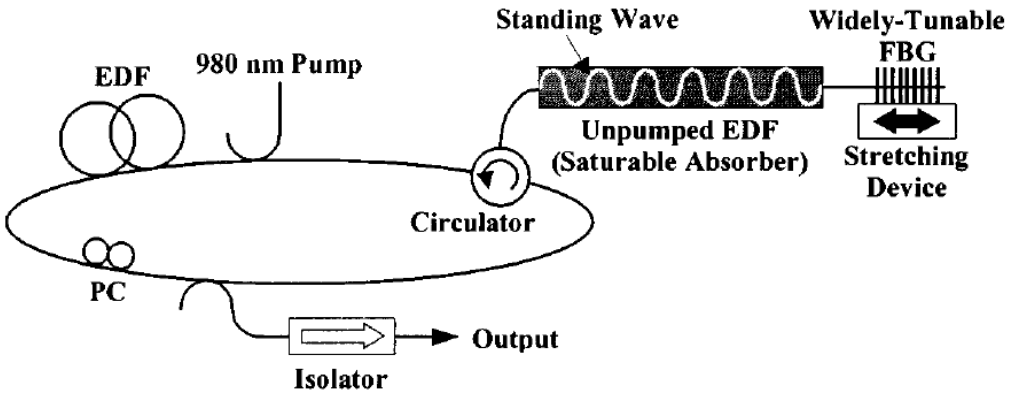

Figure 32. Tunable ring-cavity based fibre laser structure using the combination of an FBG and a saturable absorber as the wavelength selection mechanism [26].

The tunable ring-cavity based fibre laser structure, shown in Fig. 33, which employs a liquid crystal filter (LCF) as the wavelength discrimination device, has been reported and experimentally demonstrated [27]. The LCF was driven by an alternating current (AC) which caused the liquid crystal molecules to change their positions and orientations, hence changing the effective refractive index of the LCF and inducing a phase shift to the incoming light. The LCF acted as a tunable narrow band optical filter of 0.4 nm bandwidth, and the tunable fibre laser attained a total tuning range of 60 nm.

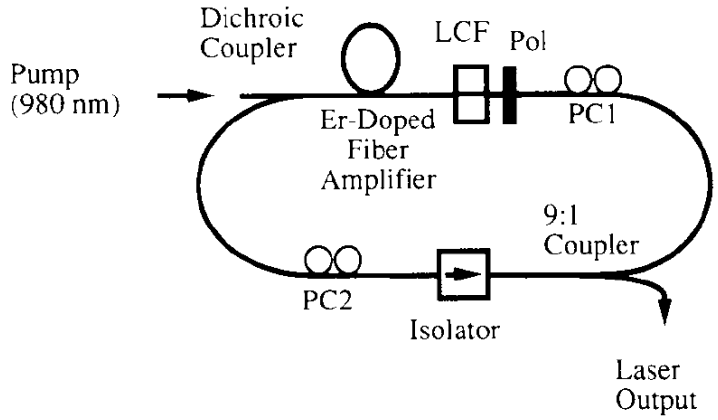

Figure 33. Tunable ring-cavity based fibre laser structure using a LCF as the wavelength selection mechanism [27].

Another tunable ring-cavity based fibre laser structure which experimentally demonstrated laser mode filtering was reported in [28]. This tunable fibre laser comprises two ring-cavities, a main ring and a sub-ring as shown in Fig. 34. Since both rings have different free spectral ranges (FSRs), due to different physical lengths, namely 16 m for the main ring and 2.1 m for the sub-ring, better mode filtering was achieved. As well, a fibre Fabry-Pérot tunable filter (FFP-TF) was employed for mode selection and an external tunable laser source was incorporated for stabilising the wavelength selected for lasing.

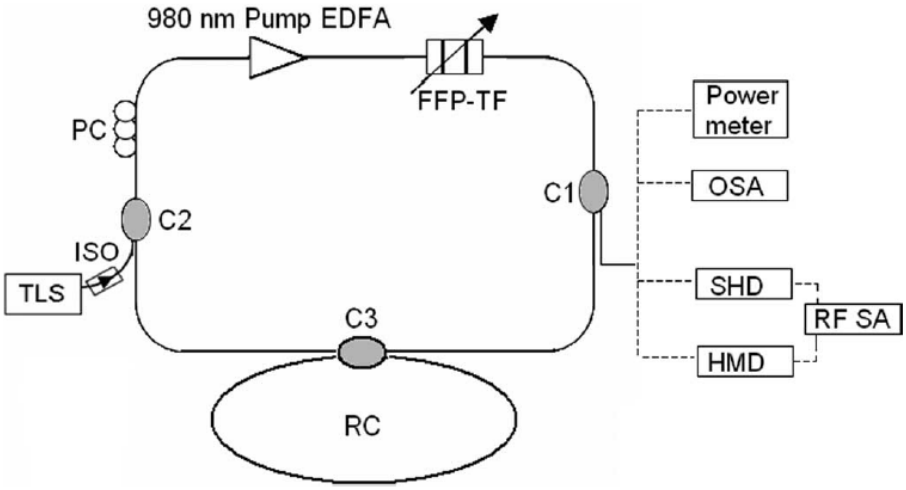

Figure 34. Tunable dual ring-cavity based fibre laser structure [28]. A FFP-TF was used for fine wavelength tuning and an external tunable laser source (TLS) was employed to increase the intensity of the lasing wavelength over the other longitudinal modes.

3.4 Conclusion

In this chapter, a literature review has been presented which described the two reported tunable fibre laser architectures based on the use of linear- and ring-cavities. The key parameters and specifications as well as the advantages and disadvantages of various reported tunable fibre laser structures have been discussed to illustrate the different methods that can be used to realise wavelength tunability.

Chapter 4

A Linear-Cavity Tunable Fibre Laser with a Saturable Absorber

4.1 Introduction

In Chapter 3, a review of the scientific literature was presented showing the reported methods to accomplish wavelength tunability in tunable fibre lasers using ring- or linear-cavities. The most common techniques reported for wavelength selection were fibre Bragg gratings (FBGs), acousto-optic filters and Fabry-Pérot filters. In this chapter, we propose and demonstrate a simple and cost-effective solution based on the use of a linear-cavity (acting as a resonant cavity) in conjunction with a saturable absorber (SA), for suppressing noise fluctuations generated in the gain medium, which create mode competition in fibre lasers, and lead to unstable laser output. Experimental results show that by optimising the length of an un-pumped erbium-doped fibre (which acts like a SA) inserted within the lasing cavity, mode competition can significantly be suppressed, thus resulting in a single lasing wavelength being amplified by the gain medium.

4.1.1 Saturable Absorber Optimisation

Various experimental procedures have been carried out to investigate how noise fluctuations that originate from high optical pumping power can be removed from a fibre laser's output. While the use of high pump power increases the laser output power, the noise fluctuations induced by mode competition degrades the stability of the lasing wavelength, leading to poor laser performance. This mainly occurs while utilising double optical pumping scheme when a standing wave pattern along the gain media is created by the two high-power signal waves travelling in opposite directions. This standing wave is the cause of spatial hole burning (SHB), which alters the gain spectrum of the optical gain medium. Once SHB is present in the gain media, different wavelengths do not experience the same amount of optical gain, leading to mode competition since the amount of energy available for the amplification of the different wavelengths is no longer constant, in comparison with the case when the gain medium is not optically pumped.

One of the methods that can help to control the noise fluctuations is the use of a section of un-pumped erbium-doped fibre (EDF), which acts as a SA when inserted into the linear resonator cavity. The aim of the SA was to behave like a narrow band filter rejecting unwanted wavelengths from amplification in the resonator cavity. This was achieved by forming constructive interference along the length of the SA, leading to a change in its refractive index, and hence creating a Bragg grating that acts as a narrow band filter with a centre wavelength equal to the lasing wavelength (as other wavelengths have lower power and experienced higher absorption than the lasing wavelength). It is important to optimise the properties of the SA in order to successfully suppress the noise fluctuations [29].

The typical location of the SA in the fibre laser system is outside the gain cavity as shown in Figure 35. This particular location of the SA is also chosen to be outside the optical pumping zone in order to form a standing wave pattern that filters the laser signal only.

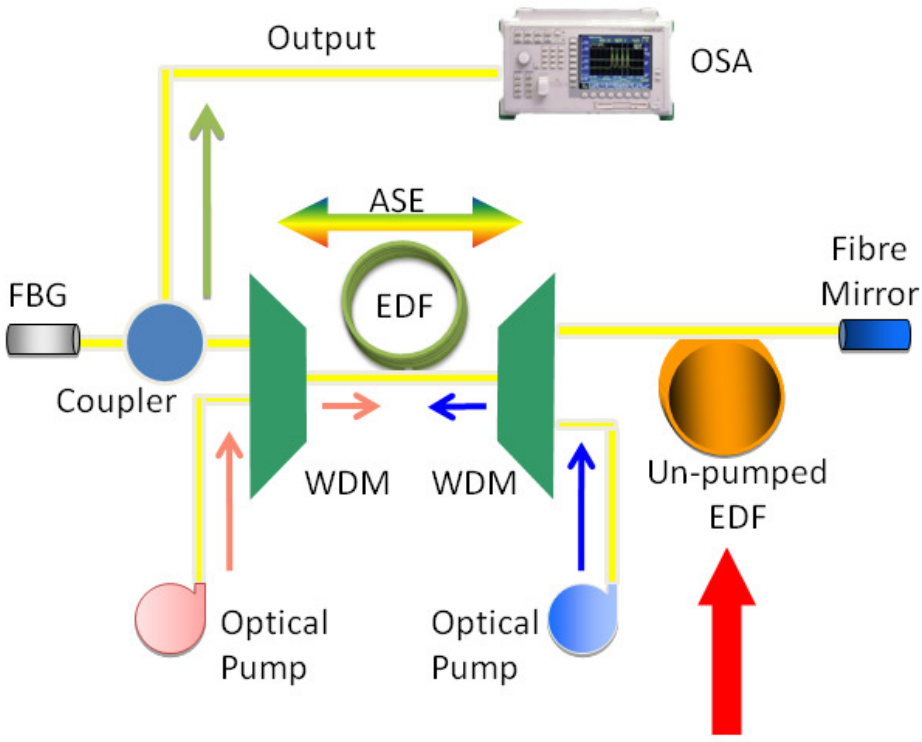

Figure 35. A double-pumped linear-cavity fibre laser with an un-pumped EDF used as a SA. The red arrow illustrates the location for the SA that suppresses noise spikes created by the high optical pumping power.

In the layout of the double-pumped linear-cavity fibre laser shown in Fig. 35, which was experimentally set up, two optical pump sources were used, namely a 980 nm laser diode and a 1480 nm laser diode, each had a maximum output optical power of 160 mW. The optical pump signal power levels were, 150 mW for the 980 nm pump and 90 mW for the 1480 nm pump. The light from both pump diodes was launched via a 1550/ 980 nm and a 1550/ 1480 nm WDM multiplexers to ensure that both pump signals were coupled into the EDFA which had a length of 15 m, and the 1550 nm ports of the WDM multiplexers were connected to a 1538.1 nm FBG and a fibre mirror, respectively, thus creating a laser system whose lasing wavelength equals to the Bragg wavelength of the FGB. A SA was connected between the 1550/ 1480 nm WDM multiplexer and the fibre mirror to induce constructive interference between two light waves travelling in opposite directions along the fibre mirror port, thus creating a standing wave within the SA, and inducing a periodic refractive change, which acted as a narrow band Bragg filter whose centre wavelength coincides with that of the FBG [30], as illustrated in Fig. 36.

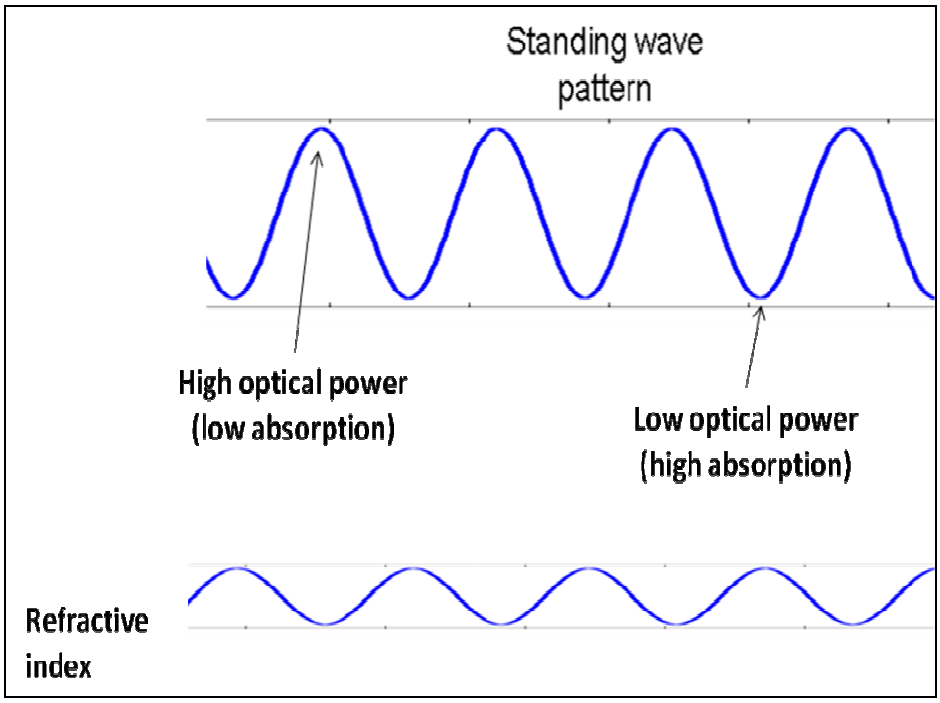

Figure 36 (a) Illustration of the standing wave pattern induced inside a SA, creating a narrow band optical filter through periodic refractive index perturbations. (b) Standing wave pattern and corresponding superposed grating due to multi-mode operation.

Controlling the bandwidth of the SA is achieved depending upon the concentration value of erbium atoms present in the doped fibre, as well as the length of the un-pumped fibre. To create a small bandwidth filter, a high doped fibre was used resulting in substantial refractive index change. The measured absorption of the saturable absorber was 6.75 dB/ m at 1532 nm.

A 5:95 fibre coupler was used to couple 95% of the lasing signal power to the FBG, which acted as one of the lasing cavity ends, while the remaining 5%, which is the laser output, was routed to an optical spectrum analyser (OSA) for laser performance monitoring.

4.2 Experimental Results

The experiments intended to demonstrate the simple yet efficient capabilities of the fibre laser to produce a stable laser output by the incorporation of a SA. By optimising the length of the un-pumped EDF, mode competition was completely eliminated and stable laser output was achieved which will be discussed later.

In a first experiment, we removed the SA and drove the pump sources until lasing took place. Figure 37 shows a snap shot generated by the OSA of the output laser spectrum. It is noticed that while an output signal at 1538.1 nm was generated, different competing longitudinal modes were also present (two of these modes are seen in the snap shot captured), resulting in an unstable output power at 1538.1 nm. The side modes resulted from the high pump power launched into the erbium-doped fibre amplifier (EDFA) and are shown in Fig. 38, which displays the measured output spectrum of the EDFA used in our experiments.

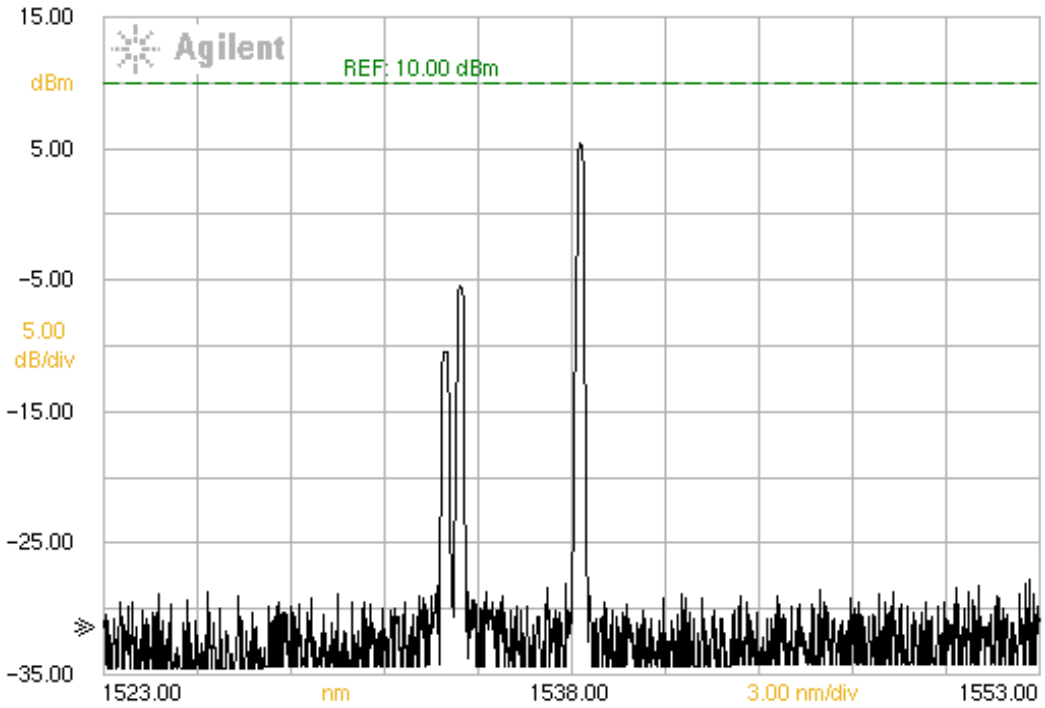

Figure 37. Measured output spectrum of the fibre laser when no SA was used. The snap shot demonstrates the presence of competing longitudinal lasing modes within the optical cavity making the output power of the fibre laser unstable.

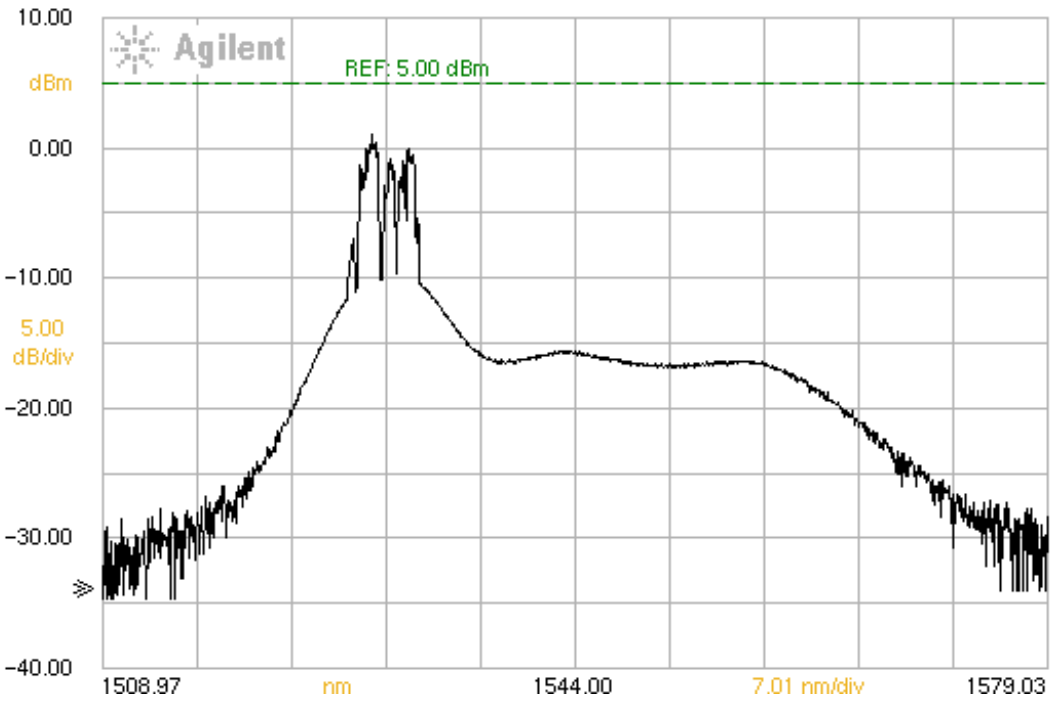

Figure 38. Illustration of measured amplified spontaneous emission (ASE) with sharp noise spikes caused by the high optical pumping power. The high pumping power is necessary in order to create an output beam with high optical power and quality shape.

In a second experiment, a 2 m long SA was used as illustrated in Fig. 35. Figure 39 shows the output spectrum of the laser system when a SA of length 2 m was used. This length was less than the optimum length, producing substantial mode competition that significantly affected the stability of the laser output. This instability in output laser power is attributed to the fact that by using the un-pumped EDF, more optical loss was introduced into the lasing cavity, thus reducing the optical power being generated at 1538.1 nm and allowing more modes to compete within the cavity. Furthermore, the several standing waves at the competing mode wavelengths are generated, thus creating a superposed grating that filters the various present modes. However, the short length of the SA results in a small refractive index contrast, and hence, week optical filtering effects that are not enough to fully suppress the competing modes. This is shown in Fig. 40, where L is the total length of the saturable absorber and Δn is the difference between the maximum and minimum changes in the refractive index of the saturable absorber.

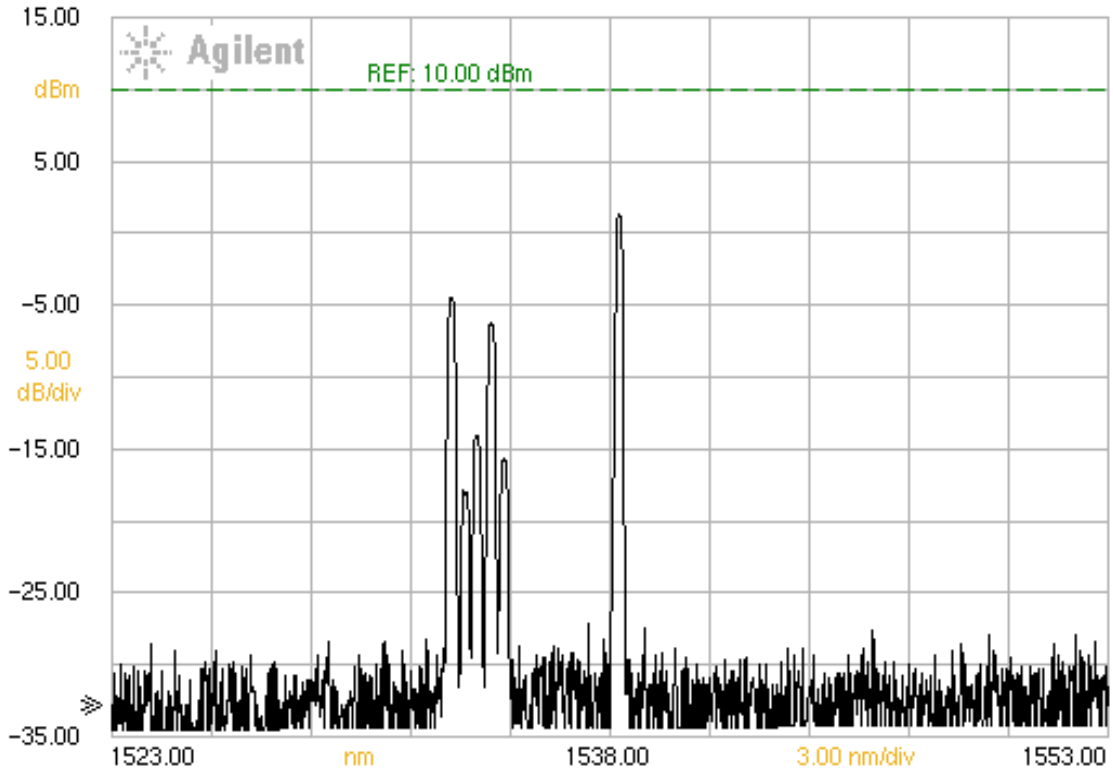

Figure 39. Measured output spectrum of the fibre laser when a 2 m long SA was used. The snap shot confirms the presence of mode competing longitudinal lasing modes within the optical cavity making the output power of the laser unstable for this length of the SA.

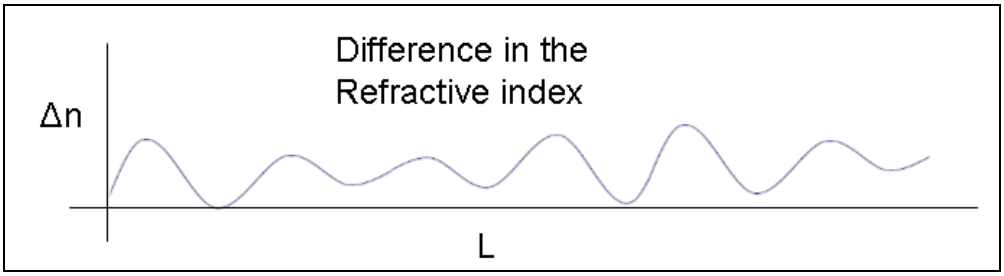

Figure 40. Refractive index differences inside the SA when no dominant mode is present, which creates a narrow Bragg grating. Since there is no periodic change in the refractive index, the resulting grating pattern allows side modes to compete within the optical cavity.

Figure 41 shows the output spectrum of the laser when the length of the SA was increased to approximately 4 m. This length was the optimum length for the SA, resulting in the superposition of several gratings with the dominant one being the grating that corresponds to the dominant mode at 1538.1 nm. All other gratings have weaker rejection effects that they do not enable other modes to lase point within the cavity. The measured full width at half maximum (FWHM) linewidth of the dominant mode was less than 0.1 nm (which is the resolution of the OSA), the side mode rejection ratio (SMRR) was more than 30 dB, and the maximum output power was around +5 dBm.

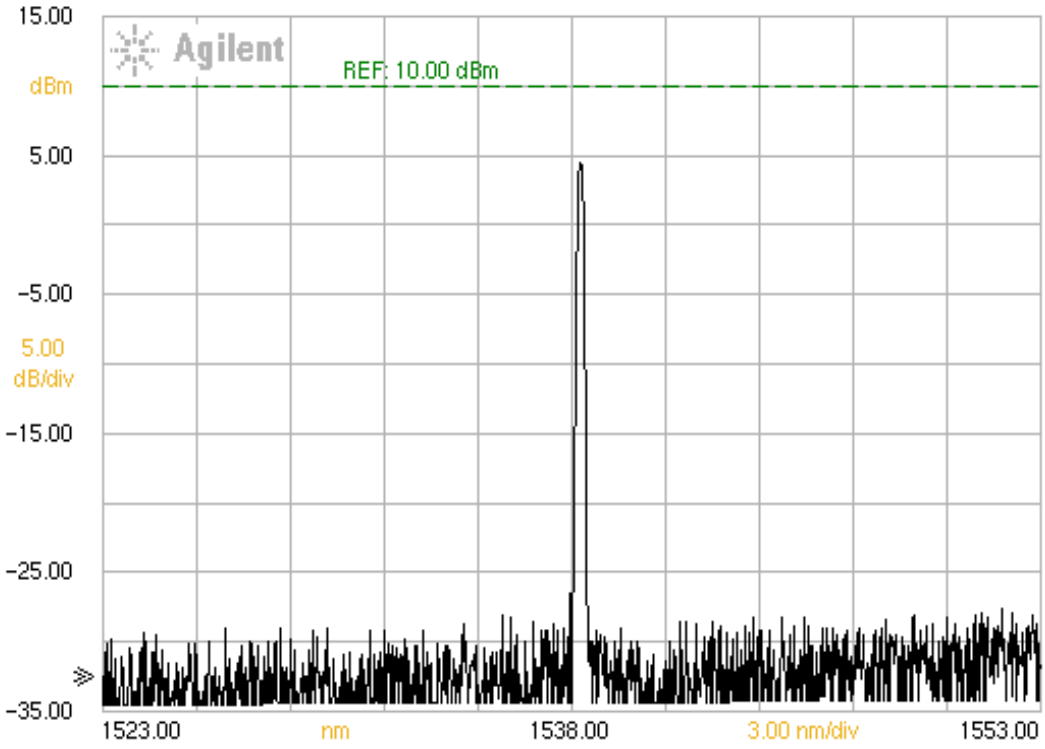

Figure 41. Laser output when the SA length was approximately 4 m which is the optimised length that minimised mode competition.

In a fourth experiment, the length of the SA was increased to 8 m. Figure 42 shows the corresponding measured output spectrum of the laser. As it can be observed, this long length of the SA not only introduced mode competition but also lowered the optimum output power by more than 3 dB. This is due to the fact that for a longer SA length the cavity loss increases thus reducing the dominant mode power as well as the power levels of the various lasing modes. This results in a standing wave pattern that corresponds to a single Bragg grating at 1538.1nm but with a weaker rejection (or broader bandwidth), thus enabling modes closer to 1538.1nm to lase, as evident from Fig. 42.

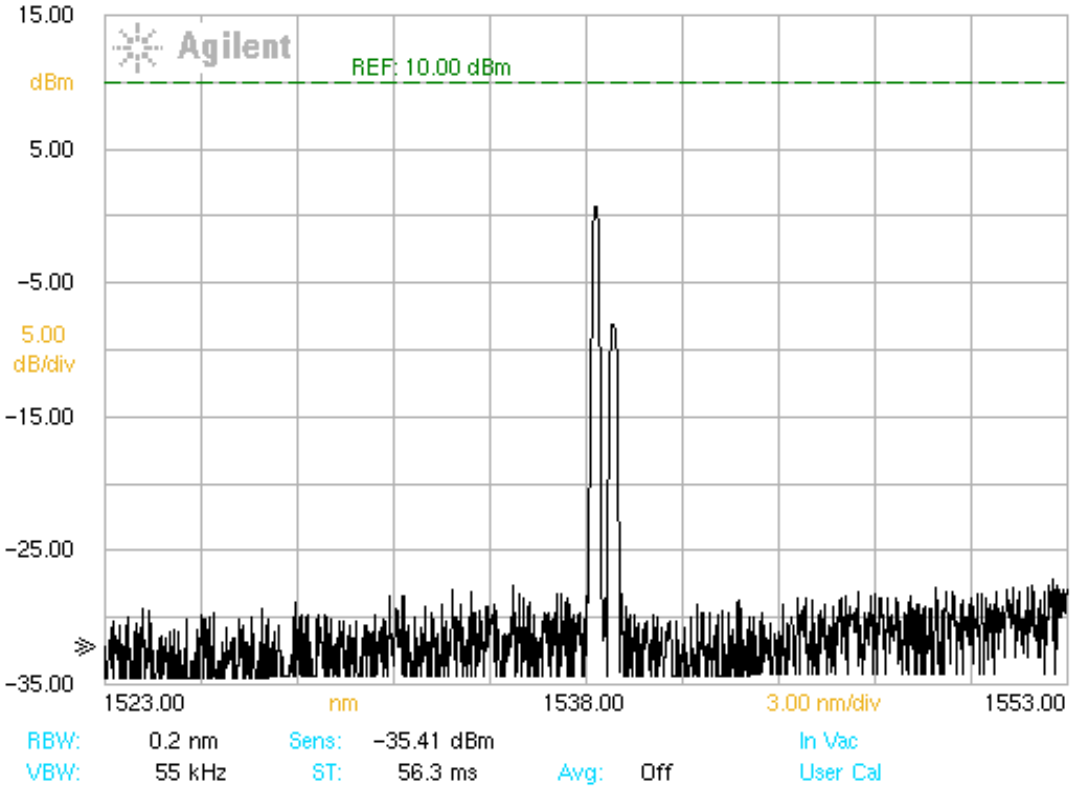

Figure 42. The output of the laser system when the length of the SA was 8 m which corresponds to more than the optimum SA length.

Note that different SA lengths within the 1-8 m range were investigated. All of them exhibited longitudinal mode generation and competition, except for the 4 m long SA. All of the results were performed at a room temperature of 23º C.

Figure 43 shows the output laser power versus the length of the SA. It is important to notice that while high output laser power is attained for a small SA length, multi-mode operation was observed, which degrades the laser performance. For an optimum SA length of around 4 m, single longitudinal mode was attained with an output laser power of around +4.5 dBm. For this SA length the noise spikes were suppressed and the output laser signal was stable for more than 10 hours.

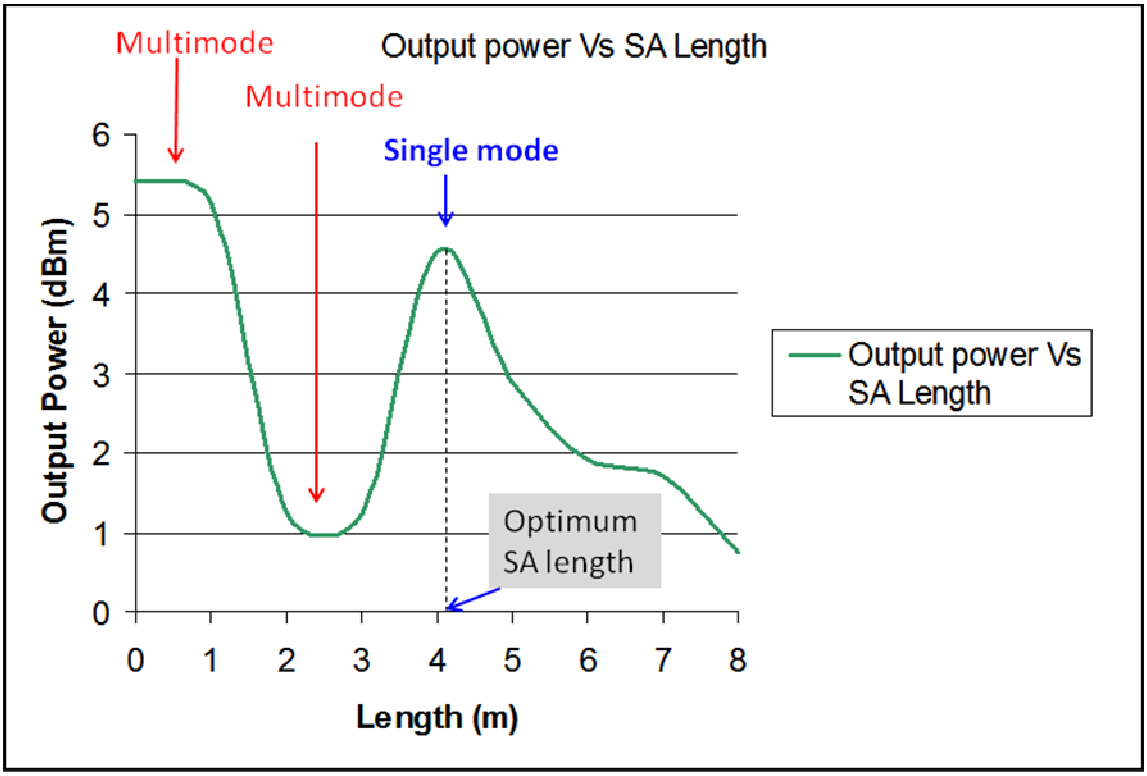

Figure 43. Relationship between the output power and the length of the SA. Optimum length of SA corresponds to highest output power at which single mode operation was attained.

4.3 Conclusions

In this chapter, experimental results have been presented, which demonstrate the capability of an un-pumped EDF to act as a SA that suppresses laser modes in a linear-cavity fibre laser. The optimum length of the SA has experimentally been evaluated, by maximising the output laser power while ensuring stable single longitudinal mode operation with suppressed noise spikes. For a dual pumping scheme employing a 150 mW 980 nm pump, a 50 mW 1480 nm pump and an EDFA length of 15 m, an optimum SA length of around 4 m has been

demonstrated to suppress noise spikes thus operating the laser in a single mode regime. The laser system has produced an optical power output of 4.5 mW with a SMRR of more than 30 dB and it has been shown that all other lengths within the tested range that do not match the optimised length of approximately 4 m for the SA result in a poor quality laser output due to the competition of various laser modes.

Chapter 5

Tunable Fibre Lasers Using a Linear-Cavity Structure

5.1 Introduction

In chapter 4, we demonstrated experimentally that incorporating a section of un-pumped erbium-doped fibre (EDF) into a linear laser cavity, stable laser output was achieved by suppressing the mode competition that is usually present when high pump power levels are used to generate high optical output laser power levels. An optimum length of the saturable absorber (SA) of around 4 m produced a single mode lasing wavelength of 4.5 mW with a side mode rejection ration (SMRR) of more than 30 dB and that all other lengths not matching the optimised length of approximately 4 m for the SA resulted in a poor quality laser output due to the competition of various laser modes. In this chapter, we propose and demonstrate the concept of two novel linear-cavity based tunable fibre laser structures employing (i) a Micro-Electro-Mechanical-System (MEMS) device and (ii) an Opto-VLSI processor, for wavelength selection, in conjunction with an erbium-doped fibre amplifier (EDFA), a fibre collimator, a Bragg grating plate and an optical lens. Experimental results demonstrate continuous tuning over the 30 nm amplified spontaneous emission (ASE) spectrum range of the EDFA, and confirm the ability of both proposed fibre laser systems to lase at any arbitrary wavelength within the available optical gain spectrum of the EDF.

5.1.1 MEMS-based Tunable Fibre Laser Employing a Linear-Cavity Structure

Figure 44 shows the layout of the proposed MEMS-based linear-cavity tunable fibre laser, which is illustrated through an experimental set up. The section of EDF acting as the gain medium had a length of 20 m and a peak core absorption of 6.5 dB/ m measured at 1530 nm. Two laser diode pumps, a 980 nm and a 1480 nm, were used for optically pumping the EDF. Each pump laser was operated at its maximum output optical power of 160 mW. The light from both pump diodes was launched via 1550/ 980 nm and 1550/ 1480 nm wave division multiplexer (WDM) couplers, respectively. A silver-coated optical fibre was used as a mirror

to create one of the cavity ends. It had an insertion loss below 0.8 dB. The laser output was extracted from the 5% port of a 5:95 fibre coupler, which was connected to the optical spectrum analyser (OSA) for wavelength and output laser power monitoring. The remaining 95% was sent to the MEMS device, which was the other reflecting end of the linear lasing cavity. A fibre based polarisation controller was used to maintain the polarisation state of the laser signal between roundtrips.

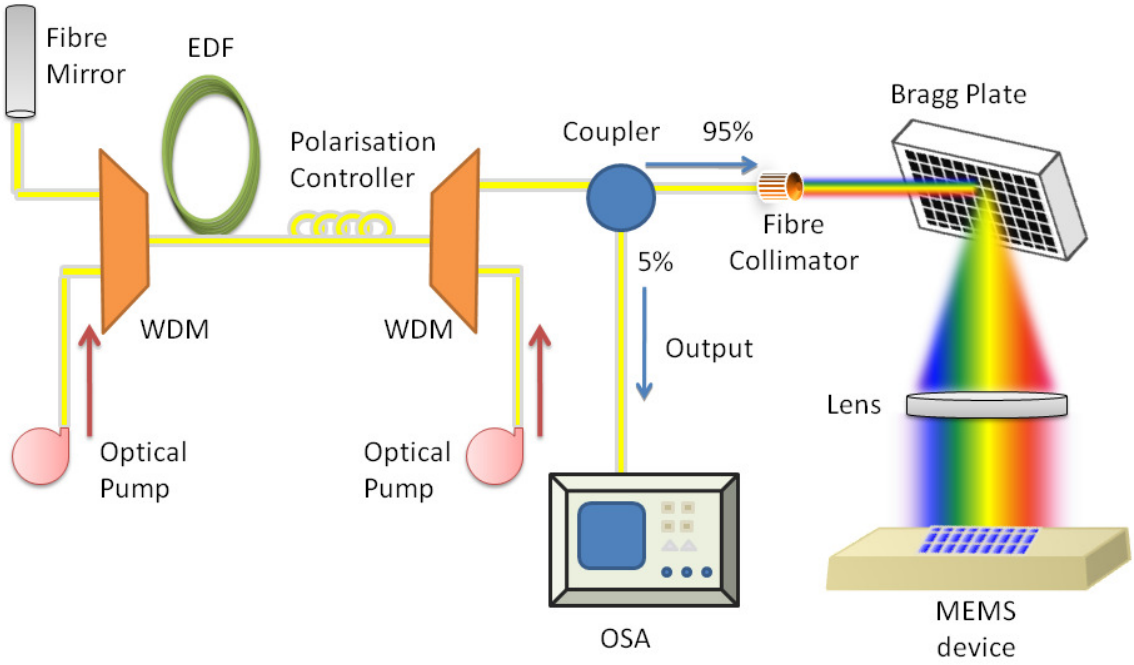

Figure 44. Experimental setup diagram for the linear-cavity tunable fibre laser structure employing a MEMS device as wavelength selection mechanism.

To achieve wavelength selection, the ASE of the EDFA was collimated at 0.5 mm diameter and mapped over the entire active window of the MEMS device, using a grating plate having 1200 lines/ mm and a blazed angle of 70° at a wavelength of 1530 nm, in conjunction with a lens of focal length 10 cm, which was placed between the grating plate and the MEMS device as shown in Fig. 45. The operating voltage of the MEMS-based device was 3.3 volts provided by the development kit's power supply.

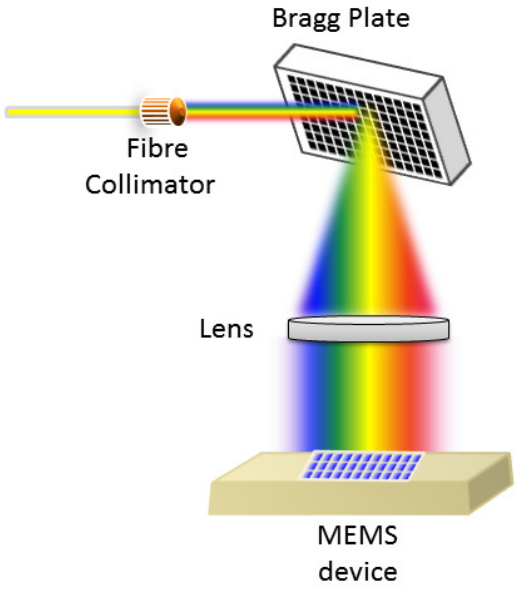

Figure 45. Illustration of the components which realise wavelength selection in the linear-cavity tunable fibre laser.

To synthesise a laser signal at a specific wavelength, λ_i, the set of micromirrors illuminated by λ_i were appropriately switched so that the incident waveband at λ_i reflected back along the same optical path and injected back into the optical cavity thus triggering laser action. This is illustrated in Fig. 46 where the selection and switching of a set of 15 micromirrors to reflect a portion of the ASE noise of the EDFA, λ_i, back into the linear-cavity to initiate laser action. The remaining energy of the ASE incident on the MEMS device was switched off-track, and hence, uncoupled back out of the fibre laser cavity. A LabView algorithm was especially developed and optimised to generate laser actions at arbitrary wavelengths, thus demonstrating a linear-cavity tunable fibre laser. The algorithm also enabled each micromirror to be treated as individual pixels.

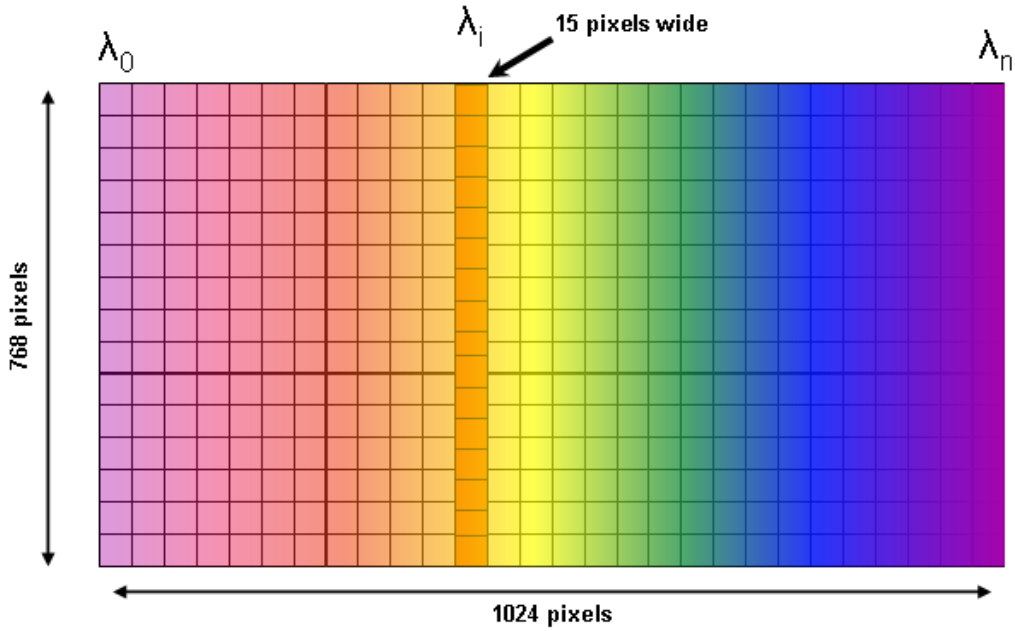

Figure 46. Illustration of the selection and switching of a set of micromirrors (orange shaded micromirrors)so that a small portion of the ASE noise of the EDFA, λ_i, was re-injected into the linear-cavity to initiate laser action.

Figure 47 shows typical laser signals generated over the complete tunable range. The measured tuning range of the laser exceeded 30 nm, which was chosen to cover the C-band telecommunications window 1530-1560 nm. The tuning resolution was 0.05 nm, which improves linearly with decreasing the micromirror size of the MEMS device. It is important to notice that the MEMS device's active window was large enough to accommodate a larger bandwidth. However, the measured range was limited because the ASE produced by the EDFA covered only the C-band. By using an optical gain medium with a broader gain spectrum EDFA a wider wavelength tuning range can be attained.

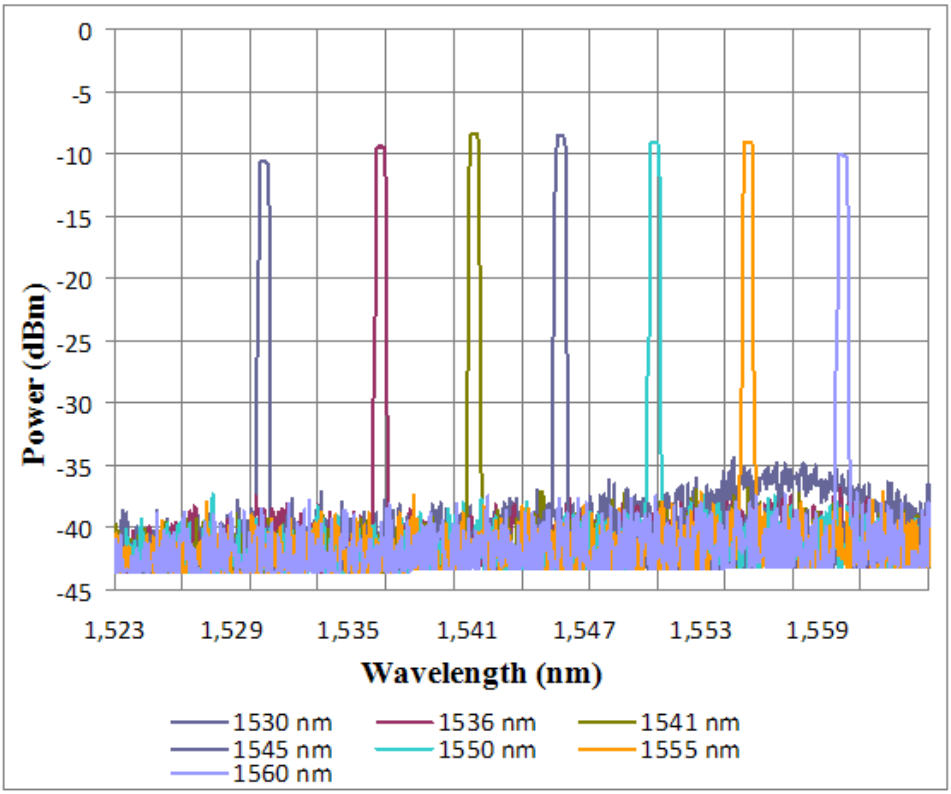

Figure 47. Typical laser signals at different wavelengths generated over a tuning range of 30 nm, using the linear-cavity tunable fibre laser demonstrator shown in Fig. 44.

Figure 47 also shows that the measured SMRR of the tunable fibre laser exceeds 30 dB throughout the entire C-Band. This makes the tunable fibre laser attractive for telecommunication applications.

5.2 OPTO-VLSI processor based Tunable Fibre Laser Employing a Linear-Cavity Structure

This section proposes and demonstrates a novel linear-cavity continuously tunable fibre laser employing an Opto-VLSI processor as the wavelength selection mechanism. The advantages of this system include (i) no mechanically moving parts, (ii) the ability to realise multiple tunable lasers using a single Opto-VLSI processor, and (iii) the ability to select any wavelength from the whole available spectrum provided from an EDF.

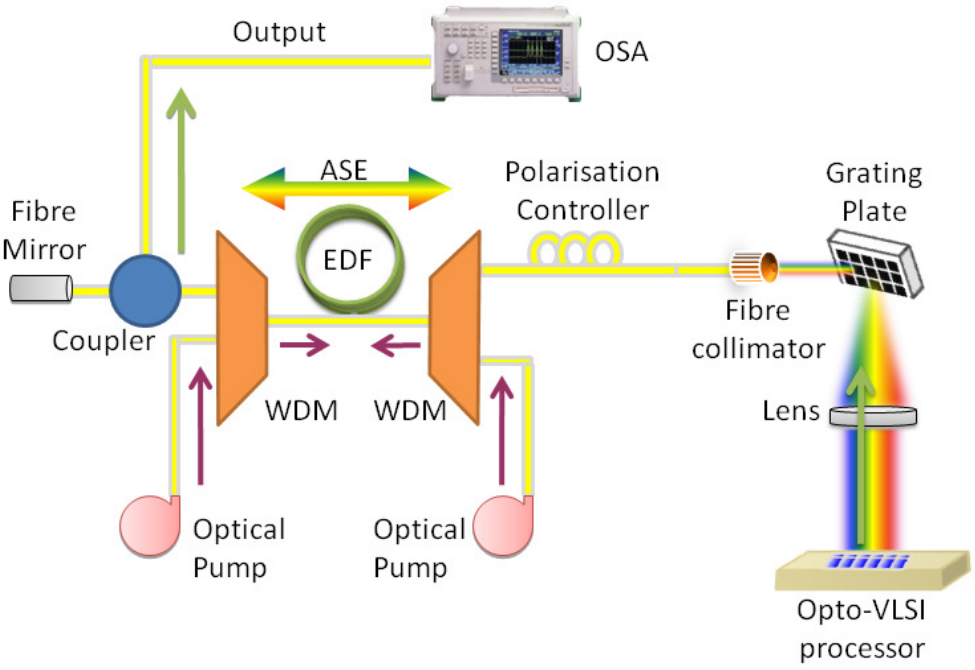

Figure 48. Architecture of the proposed fibre laser employing an Opto-VLSI processor for wavelength selection.

Figure 48 shows the layout of the proposed fibre laser, which is illustrated through the experiment that was set up. The characteristics of the EDF used in the fibre laser system were a maximum absorption value of 16 dB/ m (measured at 1530 nm), an average erbium concentration of 820 parts per million (ppm) and the length was measured to be 5 m. The ASE produced by the EDF was created by using two optical pumps which operated at 980 nm with a total maximum optical power of 160 mW each. The ASE generation was required so that the Opto-VLSI processor could select a specific wavelength for re-injection into the laser cavity for lasing. The pump light remained between two WDMs to maximise the gain media's excitation for high optical output power.

Once the selected wavelength by the Opto-VLSI processor was amplified, some of the lasing wavelength's energy was allowed to escape the resonator cavity via an optical coupler. The splitting ratio chosen for the optical coupler was 90/ 10, which relates to the amount of energy which stayed in the resonator cavity, 90%, and the remaining 10% was used as the output of the laser source. The optical coupler was used since it provided a method to tap into the resonator cavity, while minimising the resonator cavity losses, which was important in order to create a stable fibre laser output.

For the Opto-VLSI processor to accurately select the appropriate wavelength for lasing, the wavelengths in the ASE light were separated to cover the active or front window of the Opto-VLSI processor by using a Bragg reflector as illustrated in Fig. 49. Bragg reflectors are normally manufactured by creating a periodic structure on a metallic surface so that an incident broadband light beam can be reflected at different angles or orders [31]. The Bragg reflector used in the experiments had 1200 lines/ mm and high optical power for the first-order diffraction efficiency.

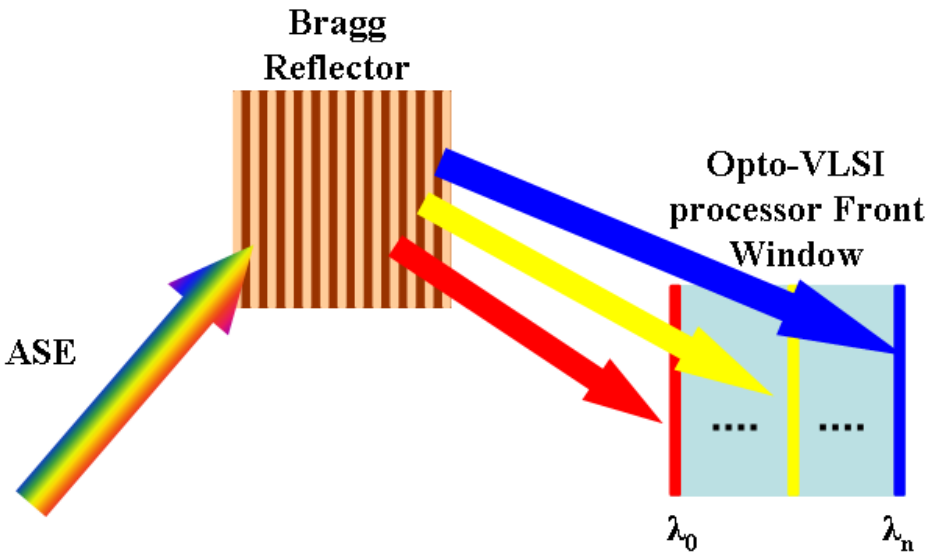

Figure 49. Broadband light beam (ASE) is separated into its individual wavelengths due to the periodic structure of the Bragg reflector. The different wavelengths then cover the front window of the Opto-VLSI processor to realise wavelength selection.

When combining the Opto-VLSI processor with a fibre collimator, grating plate and a lens, as shown in Fig. 50, an optical filter was created which enabled the selection of wavelengths within the ASE spectrum. Wavelengths within the ASE spectrum were selected without the need of scanning through the whole tunable range. This was achieved by changing the location of the user generated digital phase hologram via the software interface developed with LabView. Digital phase holograms were created through periodic voltage profiles of 10 × 512 pixels in size and with a total of 256 voltage levels.

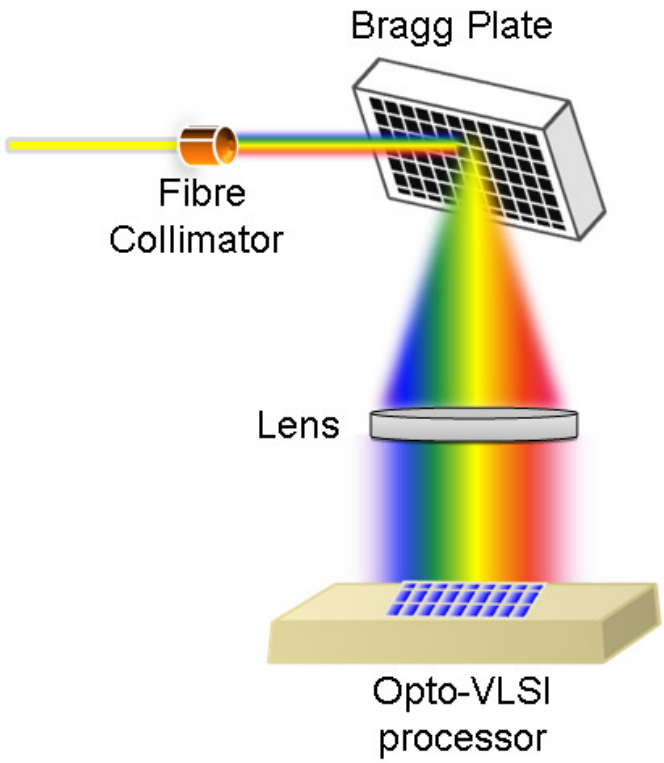

Figure 50. Illustration of wavelength selection using an Opto-VLSI processor in conjunction with various optical components to realise wavelength selection.

Patch cables were used to connect fibre components together or to extend the length of optical fibres. The specifications for a typical patch cable were (i) single mode optical fibre, (ii) angled physical contact (APC) or with straight physical contact (PC) connectors, (iii) a core diametre of 9 μm, (iv) a cladding diametre of 125 μm, (v) input loss of 0.23 dB, (vi) return loss of 52.6 dB and (vii) average length of around 1.5 m.

The polarisation controller was also an important device, which aided in controlling the polarisation state of the light inside the optical fibre. Due to the imperfections in the manufacturing process of optical fibres, the level of birefringence changes along the length of an optical fibre due to either mechanical stress or thermal effects generated by the surrounding environment where the optical fibre was being utilised. Figure 50 illustrates the polarisation controller that was employed which had three wave paddles, two 1/4 wave and a 1/2 wave, which were freely able to rotate in any direction along the optical fibre axis. The first 1/4 wave paddle changed any polarisation state into linear polarisation which then allowed the 1/2 wave paddle to change the angle of the polarisation so that the final 1/4 paddle could convert the linear polarisation to a different state of polarisation such as elliptical [32].

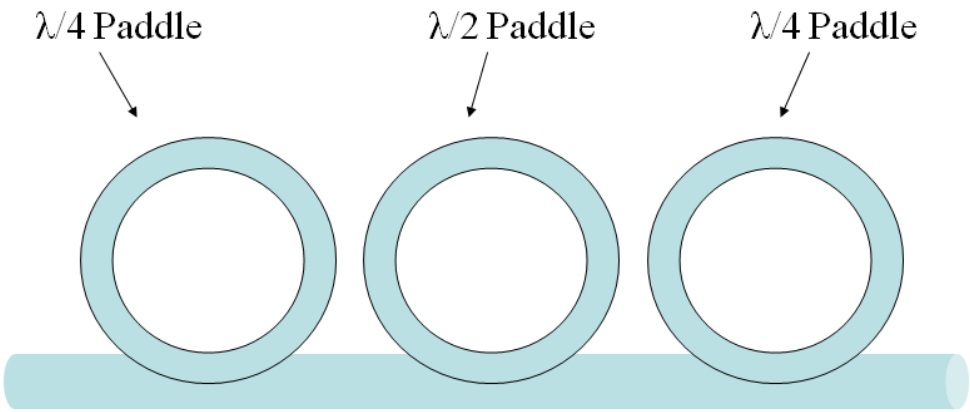

Figure 50. Fibre based polarisation controller with two 1/4 wave paddles and one 1/2 wave paddle which enable to change the state of polarisation of the light inside of an optical fibre.

5.3 Opto-VLSI processor based Tunable Fibre Laser - System Tunability

The fibre laser system was able to continuously tune wavelengths along the C-band, which corresponds to the emission spectrum of the optically-pumped EDF. The Opto-VLSI processor used a 10×512 pixel hologram which corresponded to the smallest hologram width that allowed lasing to occur. Figure 51 shows a selection of wavelengths recorded with an OSA which the fibre laser system was able to select by changing the location of the hologram on the Opto-VLSI processor. The total tuning range was measured to be more than 30 nm, from approximately 1530 nm to 1560 nm, and any wavelength within this range could be selected for lasing. It is obvious from Fig. 51 that the optical signal power decreased slightly as the wavelength was tuned far from the centre of the C-Band, however, the ASE noise around that channel also dropped, thus maintaining the SMRR around 30 dB. By increasing the pump power, a higher signal level and a higher SMRR (> 30 dB) were observed, as illustrated in Fig. 52.

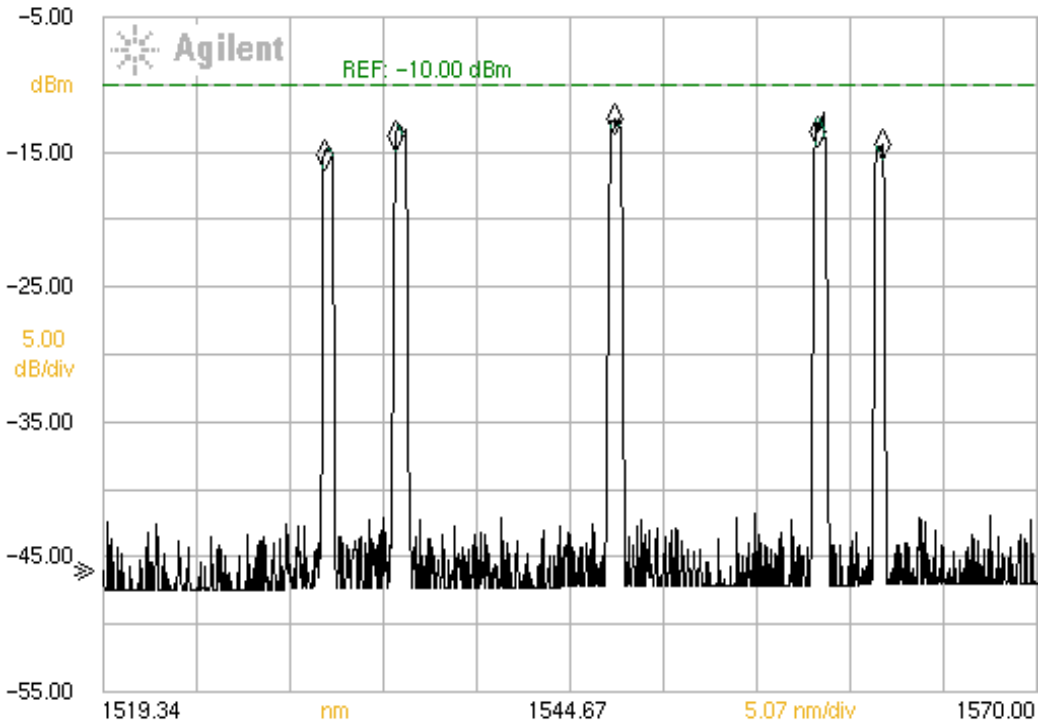

Figure 51. Range of wavelengths which the fibre laser system can select from. The different lasing wavelengths were individually generated, but they were combined onto a single diagram for simplification.

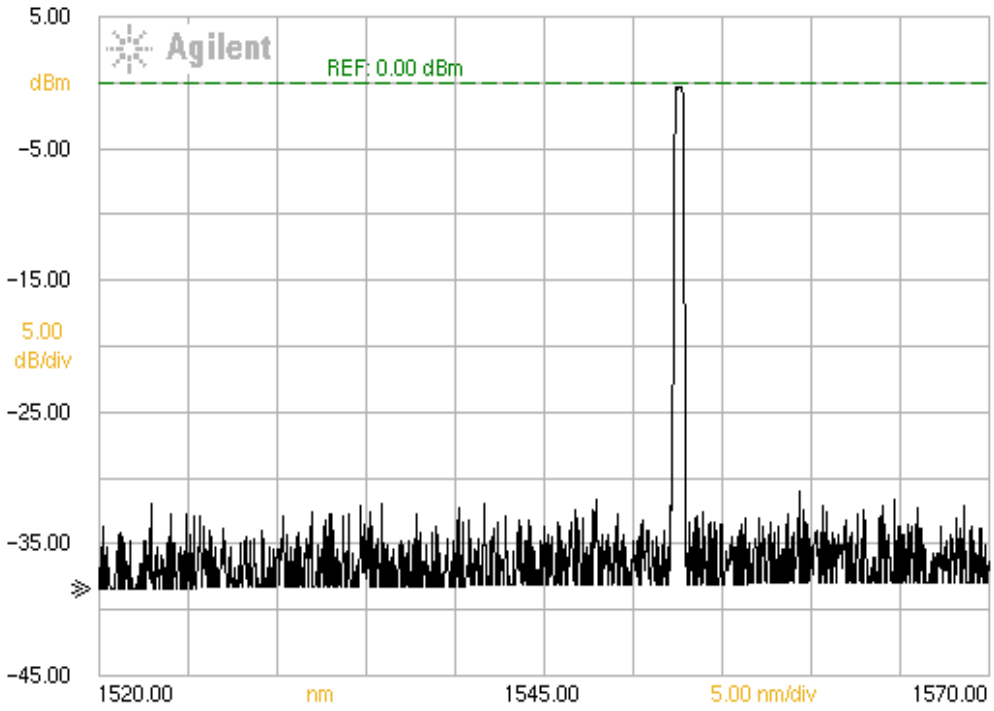

Figure 52. Data captured from the OSA of a typical lasing wavelength with a SMRR of more than 30 dB when the optical pumping power is increased producing a lasing wavelength with higher optical power than in Fig. 51.

5.4 Conclusions

In this chapter, we have experimental demonstrated the principles of two tunable fibre lasers using linear-cavities in conjunction with a MEMS device and an Opto-VLSI processor. We have shown that by electronically reconfiguring the MEMS device continuous laser wavelength tuning can be achieved over the optical amplifier gain spectrum. Experimental results have shown that the tunable fibre laser can be tuned over the entire C-band and realising a SMRR of more than 30 dB. Also, the Opto-VLSI processor has been reconfigured electronically to allow the fibre laser system to continuously tune through the available ASE spectrum of 30 nm and to select the desired wavelength for further amplification. For low optical pump powers (or gains), the Opto-VLSI processor has been able to select and re-inject wavelengths for amplification into the lasing linear-cavity, while maintaining a high SMRR exceeding 30 dB.

Chapter 6

Tunable Fibre Laser Using a Ring-Cavity Structure

6.1 Introduction

In Chapter 5, the concept of two novel linear-cavity based tunable fibre laser structures was proposed and demonstrated which employed (i) a Micro-Electro-Mechanical-System (MEMS) device and (ii) an Opto-VLSI processor, for wavelength selection, in conjunction with an erbium-doped fibre amplifier (EDFA), a fibre collimator, a Bragg grating plate and an optical lens. Experimental results demonstrated continuous tuning of 30 nm and proved the ability of both proposed fibre laser systems to lase any arbitrary wavelength within the available optical gain spectrum of the erbium-doped fibre (EDF). In this chapter, a MEMS-based tunable fibre laser using a ring-cavity is experimentally set up to compare its performance with that of the MEMS device tunable fibre laser employing a linear-cavity, which was reported in Chapter 5. Experimental results confirm that the linear-cavity fibre laser exhibits higher gain efficiency, higher laser optical output power and narrower linewidth than a ring-cavity tunable fibre laser.

6.1.1 MEMS-based Tunable Fibre Laser Using a Ring-Cavity Structure

A tunable fibre laser employing a ring-cavity structure which is illustrated in Fig. 53 was especially developed to compare the performance of the proposed linear-cavity based tunable fibre laser with that based on a ring-cavity structure. The key difference between the ring-cavity and the linear-cavity structures was that the fibre mirror used in the linear-cavity resonator was replaced by a single-mode patch cable optical fibre which was connected to an optical circulator. These components were placed between the optical coupler and the fibre collimator, to ensure uni-directional propagation of the selected wavelength for amplification in the EDF gain media. An EDF with the following properties was used as the gain medium which had 15 m in length and its peak core absorption measured at 1530 nm was 6.5 dB/ m. The optical pumping of the gain media was produced by using two pump sources, a 980 nm and a 1480 nm, each with a maximum optical power of 160 mW. In order to control the polarisation of the ASE, a polarisation controller was inserted in between two wave division

multiplexers (WDMs) which restricted the pump energy from leaving the gain media. To accurately map all of the ASE onto the MEMS device, a collimator, a Bragg plate and a lens were utilised. The collimator had a collimated beam diametre of 0.5 mm, the Bragg plate was selected due to its 1200 lines/ mm with a blaze angle of 70° measured at 1530 nm and the focal length of the lens was 10 cm. During the experiment, an optical fibre coupler was used which allowed 95% of light to reach the MEMS device for wavelength selection. The remaining 5% of light was sent to an OSA for wavelength quality monitoring.

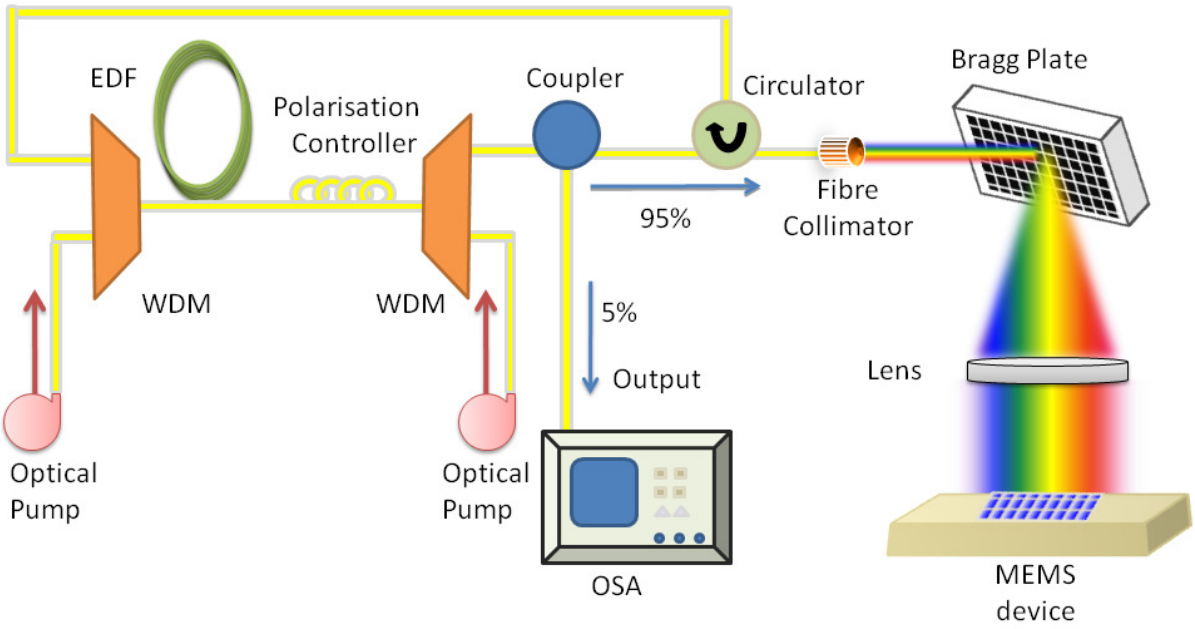

Figure 53. Experimental setup diagram for the tunable fibre laser using a ring-cavity structure and employing a MEMS device for wavelength selection.

Figure 54 shows typical laser signals generated over a wavelength range of 30 nm by the ring-cavity tunable fibre laser. The tunable range corresponds to the number of different wavelengths which a tunable laser can select for lasing. The optical pump power was 160 mW for each pump source. The side mode rejection ratio (SMRR) for the ring-cavity over the whole of the tunable range was between 15–22 dB. Also, the measured overall power differences between lasing wavelengths were around 6 dBm. The tuning range during the experiments was measured to be greater than 30 nm which corresponded to the C-band.

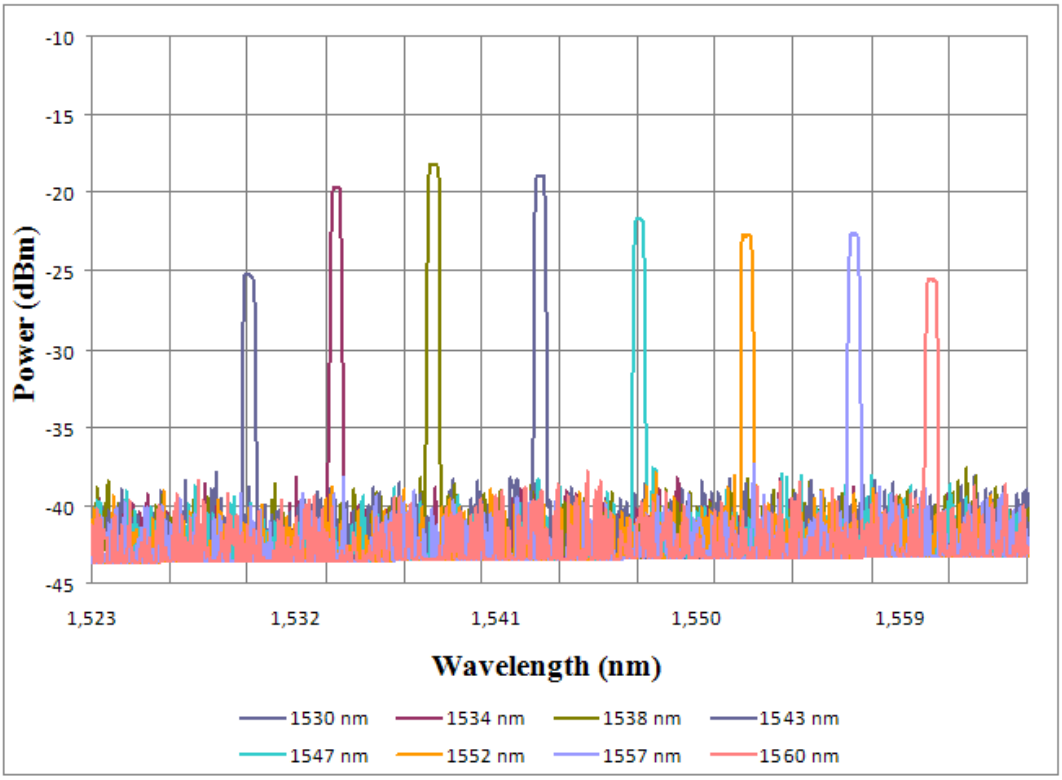

Figure 54. Typical laser signals at different wavelengths generated using the ring-cavity tunable fibre laser demonstrator shown in Fig. 53. The measured tuning range was 30 nm which covered the entire C-band.

Another characteristic of the tunable fibre laser was investigated, namely the linewidth of a typical lasing wavelength, to find out its quality. The result of a typical laser signal generated by the tunable fibre laser employing a ring-cavity structure is shown in Fig. 55. The linewidth of the ring-cavity was measured with an optical spectrum analyser (OSA) to be 0.07 nm for a lasing wavelength corresponding to 1543 nm. This wavelength of 1543 nm was found to be equal to the highest output power from the tunable fibre laser using a ring-cavity structure and was selected since it would guarantee the smallest linewidth. A comparison between the typical lasing linewidths between the ring- and the linear-cavity will be presented in the next section which will demonstrate the increased performance qualities of the linear-cavity over the ring-cavity structure.

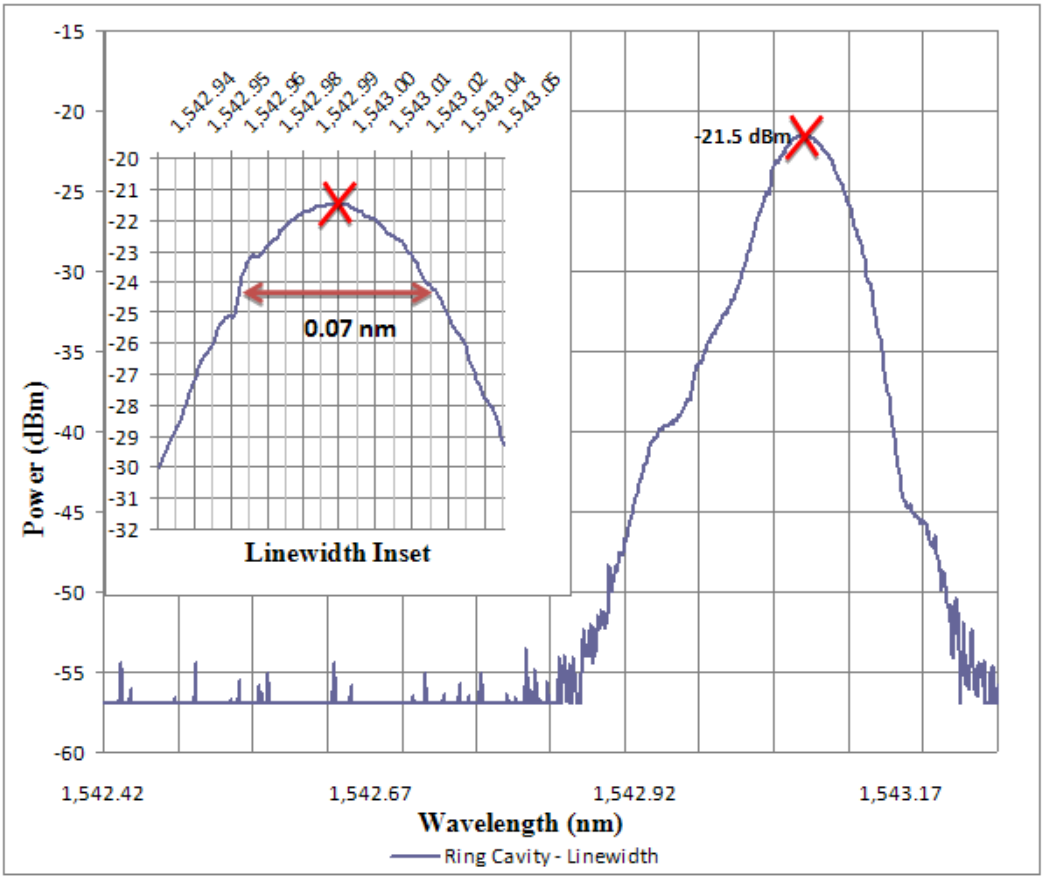

Figure 55. A typical laser signal generated by the ring-cavity fibre laser corresponding to a wavelength of 1543 nm. Expanded plot (inset) demonstrates a measured full width at half maximum (FWHM) linewidth of 0.07 nm.

6.2 Comparison Between the Linear-Cavity Tunable Fibre Laser and a Ring-Cavity Tunable Fibre Laser

This section will compare the different characteristics between ring- and linear-cavity resonant geometries for the proposed tunable fibre laser structures. As mentioned in previous chapters, the tunable fibre laser employing a linear-cavity architecture is capable of using the gain medium more efficiently, resulting in a higher quality lasing wavelength, meaning a lasing wavelength with narrower linewidth and more optical power than by using a ring-cavity structure.

The optical power between the ring- and linear-cavities will be analysed first and then the linewidth measurements will be discussed later. Figure 56 shows the maximum optical power for a typical lasing wavelength employing the linear-cavity structure which was measured to be around -9 dBm. Also, the overall power difference throughout all the tunable range was measured to be less than 3 dBm, with a SMRR of more than 30 dB.

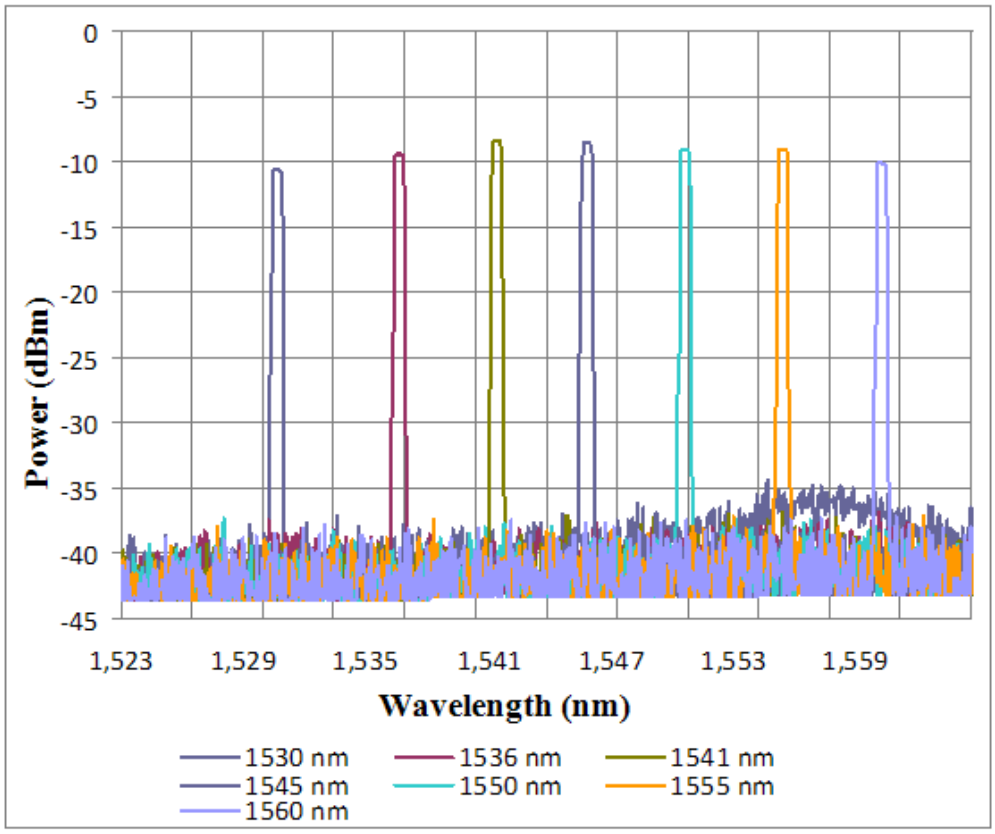

Figure 56. Typical lasing wavelengths from the tunable fibre laser using the linear-cavity structure. The maximum optical power was recorded to be -9 dBm with a SMRR of more than 30 dB.

Figure 57 shows typical lasing wavelengths from the tunable fibre laser employing a ring-cavity structure. The maximum optical power was measured to be -18 dBm, with an overall power difference of approximately 6 dBm and a SMRR of more than 20 dB. These results with the results from the linear-cavity of a maximum output power of -9 dB, an overall power difference of less than 3 dB and a SMRR of more than 30 dB, demonstrate the superior characteristics of the tunable fibre laser employing the linear-cavity structure over a ring-cavity shape.

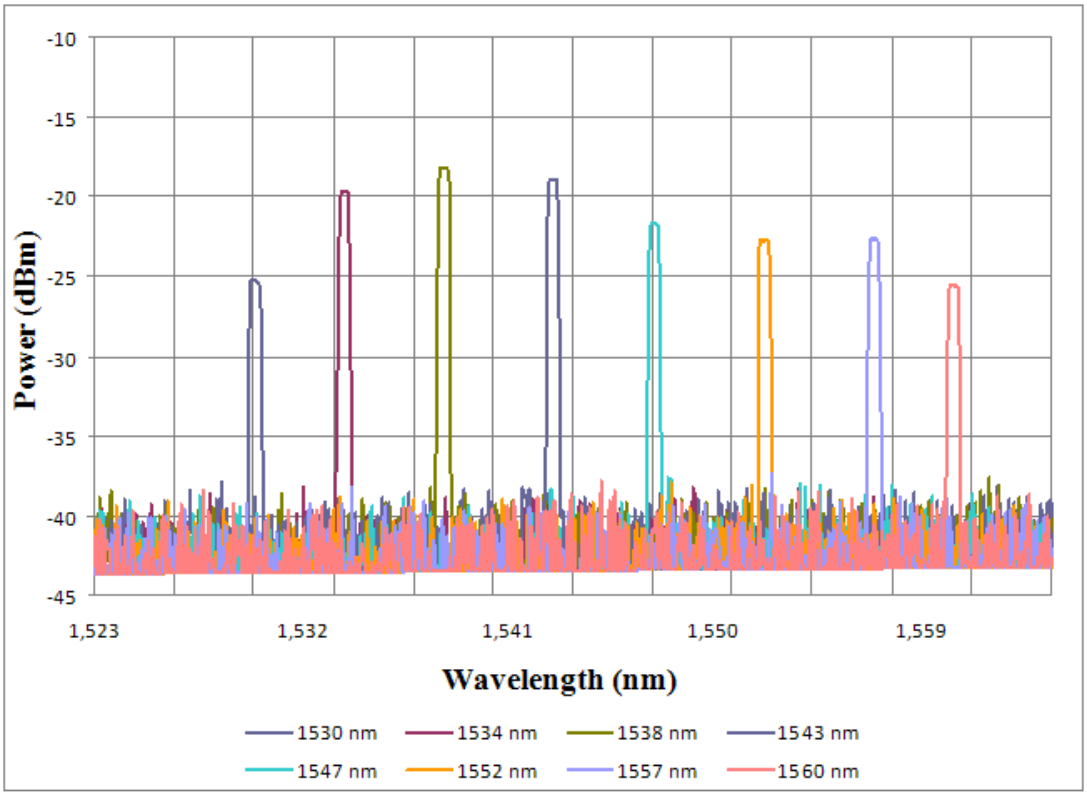

Figure 57. Typical lasing wavelengths from the tunable fibre laser using a ring-cavity structure. Maximum optical power was recorded to be -18 dBm with a SMRR of more than 20 dB.

The tunable fibre laser using a liner-cavity structure creates a self-filtering effect, enabling the lasing wavelength to experience narrower linewidths than when using a ring-cavity architecture. The linewidth for a typical lasing wavelength from the tunable fibre laser employing a linear-cavity structure is shown in Fig. 58. The linewidth was measured to be 0.06 nm corresponding to the lasing wavelength of 1541 nm. This wavelength matched the highest optical power which ensured the narrowest linewidth realisable by the tunable fibre laser employing a linear-cavity structure. Also, the linewidth of the linear-cavity equalled to that of the resolution bandwidth of the OSA used in the experiments. The resolution bandwidth is defined as the smallest possible frequency which a device can successfully evaluate. So, we believe that the actual linewidth of the linear-cavity tunable fibre laser is much smaller due to the self-filtering effect caused by the double-pass of the laser signal through the EDFA optical gain medium.

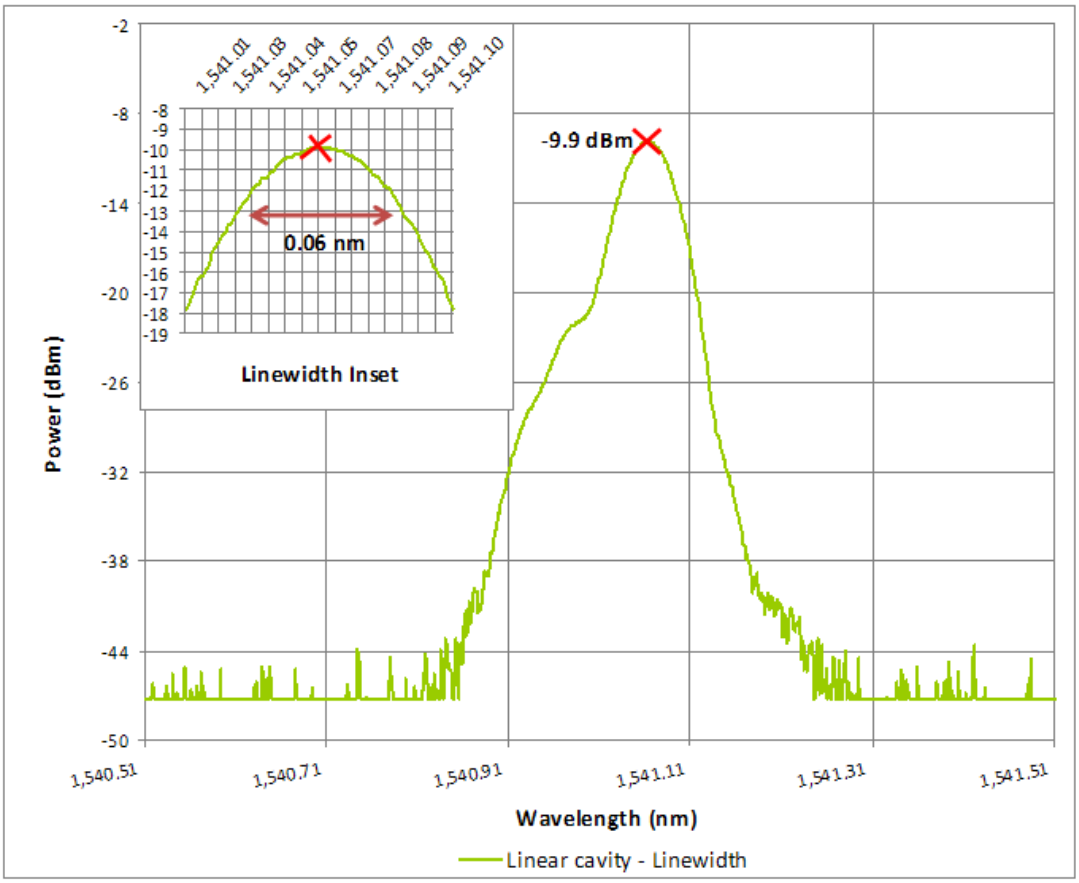

Figure 58. A typical laser signal generated by the tunable fibre laser employing a linear-cavity for measuring the laser linewidth. Expanded plot (inset) demonstrates a measured FWHM linewidth of 0.06 nm.

Figure 59 shows the typical linewidth produced by the tunable fibre laser using a ring-cavity structure. The measured linewidth, as shown in the expanded plot, was measured to be 0.07 nm. Hence, the tunable fibre laser employing a linear-cavity structure outperforms a ring-cavity architecture by allowing more efficient use of the gain media, a higher optical output power and a narrower linewidth for a typical lasing wavelength.

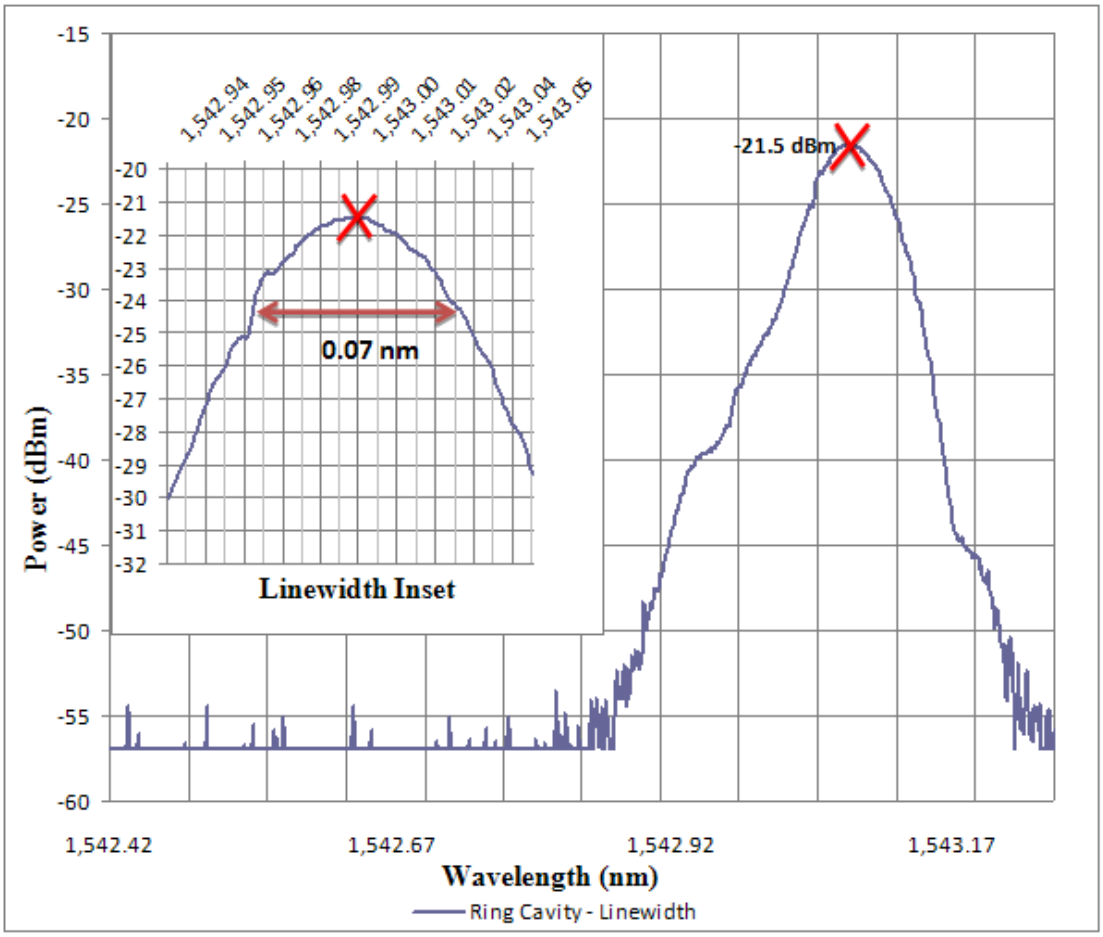

Figure 59. A typical laser signal generated by the tunable fibre laser employing a ring-cavity for measuring the laser linewidth. Expanded plot (inset) demonstrates a measured FWHM linewidth of 0.07 nm.

6.3 Conclusions

In this chapter, a ring-cavity tunable fibre laser structure has been experimentally investigated and its performance has been compared to that of the proposed linear-cavity tunable fibre laser. Experimental results have shown that while both laser structures are capable of tuning throughout the entire C-band, the linear-cavity tunable fibre laser has a linewidth below 0.06 nm, an SMRR of 30 dB and is able to generate a higher maximum output power level of -9 dBm. On the other hand, the ring-cavity tunable fibre laser has a wider measured linewidth of 0.07 nm, a lower maximum optical power of -18 dBm and a lower SMRR of around 20 dB, resulting in a laser output of inferior performance quality than the linear-cavity tunable fibre laser.

Chapter 7

Conclusion

In this thesis, tunable fibre lasers employing a linear-cavity structure and incorporating either an Opto-VLSI processor or a MEMS-based device have been proposed and demonstrated experimentally. In addition, a tunable fibre laser employing a ring-cavity structure has especially been implemented in order to compare its performance with that of the linear-cavity tunable fibre lasers. Experimental results have demonstrated that the use of a linear-cavity, rather than a ring-cavity can realise a laser with superior performance, namely higher optical output power, a higher side mode suppression ratio (SMRR) and a narrower linewidth.

In Chapter 1, the concept of lasers was presented as well as the description of the most widely used laser types, namely semiconductor lasers, gas lasers and fibre lasers. Tunable fibre lasers were presented by describing the two employed optical gain structures which are either a ring- or linear-cavity geometry. The overall system architecture for the realisation of the proposed tunable fibre laser employing a linear-cavity structure and using either an Opto-VLSI processor or a MEMS device was shown, along with a description of user generated holograms which was the main technique used to realise wavelength selection.

In Chapter 2, the main system architecture of the tunable fibre laser using a linear-cavity was presented, along with descriptions on the main benefits of using optical fibres, their physical structure and transmission modes, as well as the description of the main characteristics of the Opto-VLSI processor and the MEMS-based device used in this thesis. A list of application areas where Opto-VLSI processors and MEMS devices can be used were presented which included the telecommunications industry, spectroscopy and also as part of fibre laser sensor based devices.

In Chapter 3, a review was presented which showed the different tunable fibre laser systems that have been reported in the scientific literature. This review included ring- and linear-cavity based optical gain structures, along with the various techniques used for realising wavelength tunability. The most commonly used methods to achieve wavelength selection were stretchable fibre Bragg gratings (FBGs), acousto-optic filters and etalon based filters such as Fabry-Pérot cavities.

In Chapter 4, experimental results demonstrated the ability to suppress noise spikes produced by high optical pumping power when a section of un-pumped erbium-doped fibre (EDF) was introduced into a linear-cavity fibre laser to act as a saturable absorber (SA). When the SA had a length of approximately 4 m (corresponding to the optimised length), experimental results demonstrated that this length successfully suppressed the noise spikes resulting in a more stable laser output which did not suffer from multi-mode competition. The experimental results were performed by using an erbium-doped fibre amplifier (EDFA) length of 15 m and optically pumped using a double pump scheme, with a 980 and 1480 nm optical pumps, operating at 150 mW and 50 mW respectively. The fibre laser optical output power was measured to be 4.5 mW which corresponded to a lasing wavelength of 1538.1 nm. All of the other remaining tested SA lengths which did not correspond to the optimised length produced mode competition in the fibre laser output, resulting in a lasing wavelength with low quality performance.

In Chapter 5, two novel tunable fibre laser structures were presented which used a linear-cavity optical gain structure with the aid of an Opto-VLSI processor and a MEMS-based device to achieve wavelength tunability. The experimental results shown demonstrated the ability of the Opto-VLSI processor and the MEMS-device to be electronically reconfigured, enabling the fibre laser to continuously tune through a 30 nm range. The MEMS-based device was able to maintain a SMRR of more than 30 dB with overall optical power differences between lasing wavelengths measuring less than 3 dB. The experimental results also showed that the Opto-VLSI processor was able to select and re-inject wavelengths into the optical cavity for lasing even when the optical pumping power was reduced while maintaining a SMRR measured to be more than 30 dB throughout the entire tunable range of 30 nm.

In Chapter 6, a tunable fibre laser employing a ring-cavity structure was presented, which used a MEMS-based device for wavelength selection for comparison with the proposed linear-cavity tunable fibre laser to demonstrate the higher performance characteristics of the linear-cavity laser. The experimental results showed that the ring-cavity laser produces a similar tuning range of 30 nm to the linear-cavity. However, the maximum measured output optical power of the ring-cavity was -18 dBm, while the linear-cavity achieved a higher output optical power of -9 dBm. Also, the SMRR of the ring-cavity laser was measured to be more than 20 dB while the measured SMRR of the linear-cavity was more than 30 dB. Finally, the measured linewidth of the ring-cavity laser was 0.07 nm while the linear-cavity laser had a lower linewidth measured of 0.06 nm, demonstrating a superior performance over the ring-cavity counterpart.

7.1 Future Work

The following is a list of areas where further research has the potential to benefit the proposed and demonstrated linear-cavity tunable fibre lasers. These recommendations are after the result of numerous experiments carried out on the proposed novel linear-cavity tunable fibre lasers.

7.1.1 Gain Medium

The optical gain medium used in this project was an EDFA, which has a limited gain bandwidth product. By using an erbium-ytterbium (Er-Yr) co-doped EDFA, the gain bandwidth product of the resulting tunable laser can significantly be improved. This is also beneficial since a higher optical gain results in a narrower laser linewidth.

7.1.2 Opto-VLSI processor – Active Window

The current size of the Opto-VLSI processor's active window restricted the proposed tunable fibre laser to select wavelengths for lasing to a range matching approximately 30 nm. However, the use of a larger active window aperture will enable the proposed tunable fibre laser to select from a larger range of wavelengths, when a wideband optical amplifier is used. An Opto-VLSI processor of a larger active window enables a broader wavelength spectrum to cover the active window of the Opto-VLSI processor thus realising a wider range tunable fibre laser.

7.1.3 Multi-wavelength Generation

The generation of multiple lasing wavelengths with the aid of an Opto-VLSI processor [33] and a MEMS-based device [34] have been reported. However, all of these tunable fibre laser structures employed ring-cavities. Investigating the use of a linear-cavity tunable fibre laser to realise multi-wavelength lasing is worthwhile, as this will broaden the application areas of the proposed tunable fibre laser.

References

[1] Ali, S., Al-Khateeb, K. A. S., & Bouzid, B. (2008). Comparison of the effect structure on Ring and Linear Cavity Lasers of Er-Doped Optical Fibers. *Computer and Communication Engineering*, 546-549. doi: 10.1109/ICCCE.2008.4580663

[2] Cheng, Y., Kringlebotn, J. T., Loh, W. H. L., R.I., & Payne, D. N. (1995). Stable single-frequency travelling-wave fiber loop laser with integral saturable absorber based tracking narrowband filter. *Optics Letters*, 20(8), 875-877. doi: 10.1364/OL.20.000875

[3] Chang, S. H., Hwang, I. K., & Kim, B. Y. (2000). Widely tunable single-frequency Er-doped fiber laser with linear cavity. *Lasers and Electro-Optics*. doi: 10.1109/CLEO.2000.907366

[4] Cheng, X. P., Shum, P., Tse, C. H., Zhou, J. L., Tang, M., Tan, W. C., et al. (2008). Single-Longitudinal-Mode Erbium-Doped Fiber Ring Laser Based on High Finesse Fiber Bragg Grating Fabry–Pérot Etalon. *Photonics Technology Letters, IEEE* 20(12), 976-978. doi: 10.1109/LPT.2008.922974

[5] Zhang., J., Yue., C.-Y., Schinn, G. W., Clements, W. R. L., & Lit, J. W. Y. (1996). Stable single-mode compound-ring erbium-doped fiber laser. *Lightwave Technology*, 14(1), 104-109. doi: 10.1109/50.476143

[6] OFS. (2007). Understanding Fiber Optics: Attenuation. 3. Retrieved from http://www.ofsoptics.com/knowledge_base/search_results.php?txtProductLine=1&selCategory=1030000000086&selResource=2&txtKeywords

[7] Syms, R., & Cozens, J. (1992). *Optical Guided Waves and Devices*. London: McGraw-Hill International (UK) Limited.

[8] Hecht, J. (2006). *Understanding Fiber Optics*. New Jersey: Pearson Education, Inc., Upper Saddle River.

[9] Dammann, H. (1978). Color separation gratings. *Applied Optics, 17*, 2273-2279.

[10] Juswardy, B., Xiao, F., & Alameh, K. (2010). Opto-VLSI-based RF Beamformer for Space Division Multiple Access Network. Proceedings of International Symposium on High Capacity Optical Newtorks & Enabling Technologies. (pp. 222-226). Cairo, Egypt. IEEE.

[11] BNS Liquid Crystal Solutions. (2010, November). *Spatial Light Modulators.* Retrieved May 15, 2012, from http://www.bnonlinear.com/products/xyslm/XYSeriesDS0909.pdf

[12] Xiao, F., Juswardy, B., & Alameh, K. (2008). Opto-VLSI-based reconfigurable microwave photonic transversal filter with positive and negative coefficients. *Microwave photonics*, 251-254. doi: 10.1109/MWP.2008.4666684

[13] Alameh, K., Lee, Y. T., & Xiao, F. (2010). *Opto-VLSI-based tunable multiwavelength fiber lasers*. Paper presented at the High-Capacity Optical Networks and Enabling Technologies (HONET). http://ieeexplore.ieee.org/stamp/stamp.jsp?tp=&arnumber=5715763&isnumber=5715739

[14] Shen, M., Xiao, F., Ahderom, S., Alameh, K. (2009). An Opto-VLSI-based reconfigurable optical adddrop multiplexer employing an off-axis 4-f imaging system. *Optics Express*, 17, 14015-14022.

[15] Texas Instruments. (2010, April). *DLP® 0.55 XGA Series 450 DMD*. Retrieved, June 11, 2012, from http://www.ti.com/lit/ds/dlps013c/dlps013c.pdf

[16] Nesbitt, R. S., Smith, S. L., Molnar, R. A., & Benton, S. A. (1999). Holographic recording using a Digital Micromirror Device. *Proceedings of SPIE, 3637*. doi: 10.1117/12.343767

[17] Liu, D., Ngo, N. Q., Chan, H. N., Teu, C. K. and Tjin, S. C. (2006). A switchable triple-wavelength erbium-doped fiber laser with a linear laser cavity. *Microw. Opt. Technol. Lett.*, 48: 632–635. doi: 10.1002/mop.21429

[18] Xu, H. F., Zhan, L., Sang, M. H., Gu, Z. C., & Xia, Y. X. (2009). Switchable multiwavelength erbiumdoped fiber laser with cascaded fiber Bragg gratings and dual-section Lyot-Sagnac filter. *Modern Optics, 56*(1). doi: 10.1080/09500340802531216

[19] Song, Y. W., Havstad, S. A., Starodubov, D., Xie, Y., Willner, A. E., & Feinberg, J. (2001). 40-nm-Wide Tunable Fiber Ring Laser With Single-Mode Operation Using a Highly Stretchable FBG. *IEEE Photonics Technology Letters, 13*(11)

[20] Liu, D., Ngo, N. Q., Chan, H. N., Teu, C. K., & Tjin, S. C. (2006). A Switchable Triple-Wavelength Erbium-Doped Fiber Laser With Linear Laser Cavity. *Microwave and Optical Technology Letters, 48*(4)

[21] Stryjak, M., Budnicki, A., Lewicki, R., Kaczmarek, P. R., & Abramski, K. M. (2008). Discretely tunable and multiwavelength erbium doped fibre lasers with Fabry-Perot etalon. *Opto-Electronics Review, 16*(2), 179-184. doi: 10.2478/s11772-008-0005-4

[22] Cheng, X. P., Shum, P., Tse, C. H., Zhou, J. L., Tang, M., Tan, W. C., et al. (2008). Single-Longitudinal-Mode Erbium-Doped Fiber Ring Laser Based on High Finesse Fiber Bragg Grating Fabry–Pérot Etalon. *Photonics Technology Letters, IEEE 20*(12), 976-978. doi: 10.1109/LPT.2008.922974

[23] Chang, S. H., Hwang, I. K. K., B. Y., & Park, H. G. (2001). Widely tunable single-frequency Er-doped fiber laser with long linear cavity. *Photonics Technology Letters, IEEE, 13*(4), 287-289. doi: 10.1109/68.917827

[24] Zhou Meng; Stewart, G.; Whitenett, G. (2006). Stable single-mode operation of a narrow-linewidth, linearly polarized, erbium-fiber ring laser using a saturable absorber, *Lightwave Technology, Journal of* , *24*(5), 2179- 2183.

[25] Dong, X. (2003). Linear cavity erbium-doped fiber laser with over 100 nm tuning range. *Optics Express, 11*(14), 1689.

[26] Song, Y. W., Havstad, S. A., Starodubov, D., Xie, Y., Willner, A. E., & Feinberg, J. (2001). 40-nm-wide tunable fiber ring laser with single-mode operation using a highly stretchable FBG. *Photonics Technology Letters, IEEE, 13*(11), 1167-1169. doi: 10.1109/68.959352

[27] Maeda, M. W., Patel, J. S., Smith, D. A., Lin, C., Saifi, M. A., & Lehman, A. V. (1990). An electronically tunable fiber laser with a liquid-crystal etalon filter as the wavelength-tuning element. *Photonics Technology Letters, IEEE, 2*(11), 787-789. doi: 10.1109/68.63221

[28] Zhang, X., Zhu, N. H., Xie, L., & Feng, B. X. (2007). A Stabilized and Tunable Single-Frequency Erbium-Doped Fiber Ring Laser Employing External Injection Locking. *Lightwave Technology, 25*, 1027-1033.

[29] Meng, Z. (2006). Stable single-mode operation of a narrow-linewidth, linearly polarized, erbium-fiber ring laser using a saturable absorber. *Journal of lightwave technology, 24*(5), 2179.

[30] Horowitz, M., Daisy, R., Fischer, B., & Zyskind, J. L. (1994). Linewidth-narrowing mechanism in lasers by nonlinear wave mixing. *Opt. Lett, 19*, 1406-1408.

[31] Thorlabs. (2006). *Diffraction Grating – Tutorial.* Retrieved August 24, 2011, from http://www.thorlabs.de/tutorials/diffgratings.cfm

[32] Yao, S. (2003). The Photonics Handbook. *Polarization in Fiber Systems: Squeezing out More Bandwidth.* Laurin Publishing.

[33] Xiao, F., Alameh, K., & Lee, Y. T. (2009). Opto-VLSI-based tunable single-mode fiber laser. *Opt. Express, 17*, 18676-18680.

[34] Chen, X., Huang, K., Wang, Y., Song, F., Chen, G., Sang, X., et al. (2012). Tunable polarization-maintaining single-mode fiber laser based on a MEMS processor. *CLEO: QELS-Fundamental Science, OSA Technical Digest.*

[Figure 5] Las Cumbres Observatory Global Telescope Network. (2012). *Light as a Wave: Electromagnetic waves* [Image]. Retrieved from http://lcogt.net/book/export/html/3666

[Figure 9] Paschotta, R. (2011). *CO_2 Lasers* [Image]. Retrieved from http://www.rp-photonics.com/co2_lasers.html